

RESEARCH ARTICLE

A potent nuclear export mechanism imposes USP16 cytoplasmic localization during interphase

Nadine Sen Nkwe¹, Salima Daou^{1,2}, Maxime Uriarte¹, Jessica Gagnon^{1,3}, Nicholas Victor Iannantuono^{1,3}, Haithem Barbour¹, Helen Yu^{1,4}, Louis Masclef¹, Erlinda Fernández¹, Natalia Zamorano Cuervo^{1,5}, Nazar Mashtalir^{1,6,7}, Loïc Binan^{1,8}, Mikhail Sergeev¹, François Bélanger¹, Elliot Drobetsky^{1,9}, Eric Milot^{1,9}, Hugo Wurtele^{1,9}, Santiago Costantino^{1,8} and El Bachir Affar^{1,9,*}

ABSTRACT


USP16 (also known as UBP-M) has emerged as a histone H2AK119 deubiquitylase (DUB) implicated in the regulation of chromatin-associated processes and cell cycle progression. Despite this, available evidence suggests that this DUB is also present in the cytoplasm. How the nucleo-cytoplasmic transport of USP16, and hence its function, is regulated has remained elusive. Here, we show that USP16 is predominantly cytoplasmic in all cell cycle phases. We identified the nuclear export signal (NES) responsible for maintaining USP16 in the cytoplasm. We found that USP16 is only transiently retained in the nucleus following mitosis and then rapidly exported from this compartment. We also defined a non-canonical nuclear localization signal (NLS) sequence that plays a minimal role in directing USP16 into the nucleus. We further established that this DUB does not accumulate in the nucleus following DNA damage. Instead, only enforced nuclear localization of USP16 abolishes DNA double-strand break (DSB) repair, possibly due to unrestrained DUB activity. Thus, in contrast to the prevailing view, our data indicate that USP16 is actively excluded from the nucleus and that this DUB might indirectly regulate DSB repair.

This article has an associated First Person interview with the first author of the paper.

KEY WORDS: Deubiquitylase, Ubiquitin, USP16, UBP-M, H2AK119, Nuclear export, Cell proliferation, Mitosis, DNA double-strand break repair

¹Maisonneuve-Rosemont Hospital Research Center, Montréal, QC H1T 2M4, Canada. ²Lunenfeld-Tanenbaum Research Institute, Sinai Health System, Toronto, ON M5G 1X5, Canada. ³Institute for Research in Immunology and Cancer, University of Montréal, Montréal, QC H3T 1J4, Canada. ⁴Developmental and Stem Cell Biology Program and Arthur and Sonia Labatt Brain Tumor Research Centre, Hospital for Sick Children, Toronto, ON M5G 0A4, Canada. ⁵CRCHUM-Centre Hospitalier de l'Université de Montréal, 900 rue Saint Denis, Montréal, QC H2X 0A9, Canada. ⁶Department of Pediatric Oncology, Dana-Farber Cancer Institute and Harvard Medical School, Boston, MA 02215, USA. ⁷Broad Institute of MIT and Harvard, Cambridge, MA 02142, USA. ⁸Department of Ophthalmology, University of Montréal, Montréal, Québec, Canada. ⁹Department of Medicine, University of Montréal, Montréal H3C 3J7, Québec, Canada.

*Author for correspondence (el.bachir.affar@umontreal.ca)

 N.S.N., 0000-0002-1099-6601; S.D., 0000-0002-3473-3814; M.U., 0000-0002-0885-7063; J.G., 0000-0003-3191-5265; N.V.I., 0000-0003-3362-1690; H.B., 0000-0002-4373-3728; H.Y., 0000-0002-5948-8384; L.M., 0000-0003-3034-5758; E.F., 0000-0002-3630-7587; N.Z.C., 0000-0001-9199-9654; N.M., 0000-0002-6624-4839; L.B., 0000-0002-3886-5873; M.S., 0000-0001-7047-2378; F.B., 0000-0001-7072-7545; E.D., 0000-0002-0991-4314; E.M., 0000-0002-2851-077X; H.W., 0000-0002-5733-1711; S.C., 0000-0002-2454-2635; E.B.A., 0000-0002-6374-3683

Received 17 September 2019; Accepted 13 January 2020

INTRODUCTION

Ubiquitylation is a critical post-translational modification that regulates a myriad of signaling events and cellular processes (Gomez-Diaz and Ikeda, 2018; Grumati and Dikic, 2018; Hammond-Martel et al., 2012; Harper et al., 2018; Hu and Sun, 2016; Schwertman et al., 2016; Uckelmann and Sixma, 2017; Vucic et al., 2011; Werner et al., 2017; Wertz and Dixit, 2010). This modification is catalyzed by the concerted action of E3 ubiquitin ligases and E2 ubiquitin-conjugating enzymes, which play central roles in substrate recruitment, and in dictating the mode of ubiquitin molecule attachment, respectively (Yau and Rape, 2016; Zheng and Shabek, 2017). E3 (about 600 genes) and E2 (about 40 genes) enzyme pairs target a wide spectrum of cellular proteins, consistent with the pervasive role of the ubiquitin system in cell function and homeostasis (Clague et al., 2015). Indeed, deregulation of ubiquitin conjugation underlies numerous human pathologies, including cancer and neurodegenerative diseases (Heaton et al., 2016; Mendler et al., 2016; Popovic et al., 2014; Rubinsztein, 2006; Senft et al., 2018; Tanaka and Matsuda, 2014).

Deubiquitylation is responsible for the timely removal of ubiquitin from substrates, and as such can regulate protein function in a proteasome-dependent or -independent manner. A large superfamily of more than 100 deubiquitylases (DUBs), which are either cysteine- or metallo-proteases, are primary determinants in mediating or terminating ubiquitin signaling processes (Clague et al., 2019; Eletr and Wilkinson, 2014; Nijman et al., 2005; Reyes-Turcu et al., 2009). DUBs are critical for diverse cellular processes, including cell cycle control, membrane signaling, transcription and DNA damage/repair processes (Bonacci et al., 2018; Daou et al., 2018; Hammond-Martel et al., 2012; Hu and Sun, 2016; Jackson and Durocher, 2013; Nishi et al., 2014; Perrody et al., 2016). Moreover, DUBs are regulated at the levels of multi-protein complex assembly, enzymatic activity and subcellular localization, although their mechanisms of action are not fully understood (Clague et al., 2019; Fraile et al., 2012; Komander et al., 2009; Mevissen and Komander, 2017; Sahtoe and Sixma, 2015).

USP16 (also known as UBP-M), a widely-expressed cysteine protease of the USP family, has been implicated in the control of chromatin-associated processes, cell proliferation and differentiation (Cai et al., 1999; Joo et al., 2007; Minnaugh et al., 2001; Yang et al., 2014). Increased dosage of *USP16* (located on chromosome 21), as a consequence of gene triplication, has been shown to inhibit stem cell renewal and to promote cellular senescence, mechanisms that in turn might contribute to the pathogenesis of Down's syndrome (Adorno et al., 2013). The *USP16* gene locus is targeted by oncogenic translocations with the transcription factor RUNX1 during leukemia, suggesting that USP16 might play important roles in the hematopoietic system (Gelsi-Boyer et al., 2008). Indeed, while *Usp16* gene ablation causes embryonic lethality in mice, conditional

inactivation in the bone marrow has demonstrated that this DUB is required for proper hematopoiesis and lineage commitment of hematopoietic stem cells (HSCs) (Gu et al., 2016; Yang et al., 2014). On the other hand, USP16 is not required for renewal of embryonic stem cells, but rather regulates their differentiation (Gu et al., 2016; Yang et al., 2014).

While the importance of USP16 in pathophysiology is becoming increasingly recognized, the relationship between its subcellular localization and function remains largely unclear. Initial observations have revealed that USP16 is primarily in the cytoplasm (Cai et al., 1999; Urbé et al., 2012). Interestingly, a catalytic dead mutant of USP16 was found to be nuclear, suggesting a potential role of enzymatic activity in coordinating the subcellular localization of this DUB (Cai et al., 1999), but the significance of this event remained unexplained. Importantly, the main roles attributed to USP16 are related to nuclear processes, such as transcription and DNA repair (Frangini et al., 2013; Joo et al., 2007; Shanbhag et al., 2010; Yang et al., 2014; Zhang et al., 2014). It has been reported that USP16 deubiquitylates histone H2AK119 (hereafter H2Aub), a polycomb repressive complex 1 (PRC1)-catalyzed chromatin modification that regulates gene expression and DNA repair (Cai et al., 1999; Joo et al., 2007). Several studies have reported that USP16 depletion leads to deregulation of gene expression and that this DUB could be detected at gene regulatory regions (Gu et al., 2016; Joo et al., 2007; Yang et al., 2014). Other studies suggest that USP16 might directly regulate chromatin remodeling at sites of DNA damage (Shanbhag et al., 2010; Zhang et al., 2014). USP16 also appears to influence mitosis, as its knockdown induces G2/M delay and decreases cell proliferation (Joo et al., 2007). In addition, it has been proposed that deubiquitylation of histone H2Aub by USP16 is prerequisite for histone H3S10 phosphorylation, a chromatin modification mark associated with mitosis (Joo et al., 2007). More recently, USP16 has been shown to regulate the stability of PLK1 at kinetochores by promoting kinetochore–microtubule attachments and proper chromosome alignment (Zhuo et al., 2015).

Despite the above studies reporting that USP16 exerts important functions in DNA-associated processes, it remained largely unclear (1) how the potential import of USP16 into the nucleus regulates such processes and (2) whether the observed changes on DNA repair and gene expression are direct effects of USP16 recruitment to chromatin or an indirect consequence of its depletion or overexpression. Moreover, the molecular determinants that might regulate USP16 nuclear import or export have not been identified. For instance, systematic identification of nuclear export signals (NES) in DUBs, using multiple prediction tools, failed to reveal such motifs in USP16 (Garcia-Santisteban et al., 2012). However, preliminary results of domain mapping suggested that USP16 contains potential NLS and NES sequences (Xu et al., 2013), but the identity of genuine and transferable nuclear import and export signals in this DUB has remained elusive.

In this study, we rigorously established the subcellular localization of USP16 during cell cycle progression and identified the molecular determinants that coordinate USP16 nucleo-cytoplasmic trafficking. Our data challenge the current conclusions on USP16 function and support a model whereby cytoplasmic USP16 might indirectly regulate chromatin function in the absence of active translocation into the nucleus.

RESULTS

USP16 is predominantly cytoplasmic during interphase

To determine the relationship between USP16 localization and function, we first generated an anti-USP16 antibody and used RNAi

to validate the specific detection of endogenous USP16 by immunoblotting (Fig. S1A). Next, we conducted a hypotonic lysis-based subcellular fractionation of HEK293T and U2OS cells, and then purified nuclei through a sucrose cushion. Immunodetection of poly(ADP-ribose) polymerase 1 (PARP-1) and lactate dehydrogenase (LDH), nuclear and cytoplasmic enzymes, respectively, was conducted to control for cross-contamination of fractions. We observed that while LDH was almost completely absent from the nuclear fraction, a minor pool of USP16 remained associated with nuclei (Fig. 1A). We reasoned that either a pool of USP16 could be associated with cellular membranes and organelles that co-fractionate with the nucleus or a small fraction of USP16 might be localized inside the nucleus. To distinguish between these possibilities, we conducted immunostaining of USP16 on asynchronous cell populations. With several commercial anti-USP16 antibodies as well as one made in-house, we did not detect a specific endogenous USP16 signal in the nucleus, as the fluorescence signal in this compartment remained unchanged following USP16 depletion by siRNA (Fig. S1B,C). However, the cytoplasmic signal, detected with two commercial antibodies, significantly decreased following USP16 depletion, indicating the presence of this DUB in the cytoplasm (Fig. S1B,C). We then expressed Myc-tagged USP16 in U2OS cells through lentiviral transduction and conducted confocal microscopy, which revealed that this DUB is localized in the cytoplasm (Fig. 1B). Relative quantification indicated that the immunofluorescence signal detected in the nucleus is indistinguishable from the background (Fig. 1B). To exclude potential cell fixation artifacts, we expressed a GFP–USP16 fusion construct and monitored its subcellular localization on live cells. GFP signal quantification confirmed that GFP–USP16 is cytoplasmic with nearly undetectable levels inside the nucleus of transfected cells (Fig. 1C; Movie 1). We also did not detect USP16 in the nucleus using 3D image deconvolution (Fig. S1D). The cytoplasmic localization of USP16 is not affected by the levels of DUB expression (Fig. S1E). USP16 is also cytoplasmic in IMR90 fibroblasts transduced with GFP–USP16 (Fig. S1F). Interestingly, we occasionally observed cells with a nucleocytoplasmic staining of GFP–USP16, generally in pairs of adjacent cells (Fig. 1D). These cells have strongly reduced H2Aub signal, consistent with the ability of USP16 to deubiquitylate this histone, and are extremely rare (representing less than 1% of counted cells).

Since USP16 has been associated with cell cycle progression (Joo et al., 2007), we sought to determine whether USP16 enters the nucleus at a specific cell cycle phase. U2OS cells transfected with a Myc–USP16 expression construct were synchronized at various cell cycle phases (Fig. 1E) (Hammond-Martel et al., 2010; Vassilev et al., 2006). Flow cytometry analysis indicated that indeed cells were synchronized in the expected cell cycle phases (Fig. 1F, bottom panels). Immunofluorescence staining showed that USP16 remains cytoplasmic in the G1, G1/S, S and G2 phases (Fig. 1F, top panels). No noticeable changes in the levels of histone H2Aub were observed in the majority of USP16-transfected cells. Mitotic cells within the G2/M population (indicated by arrows) are typically round with condensed chromosomes and have low H2Aub levels. The staining of USP16 is diffuse in M phase cells, as their nuclear membranes are presumably disassembled. Interestingly, we found that the occasional presence of USP16 in both the cytoplasm and the nucleus of two adjacent cells is mostly associated with the G1 cell population (Fig. 1G). The detection of a cytoplasmic bridge, which is indicative of incomplete cytokinesis, could be occasionally detected in the two daughter cells, suggesting that these cells are in early G1. These cells have reduced H2Aub levels and their number

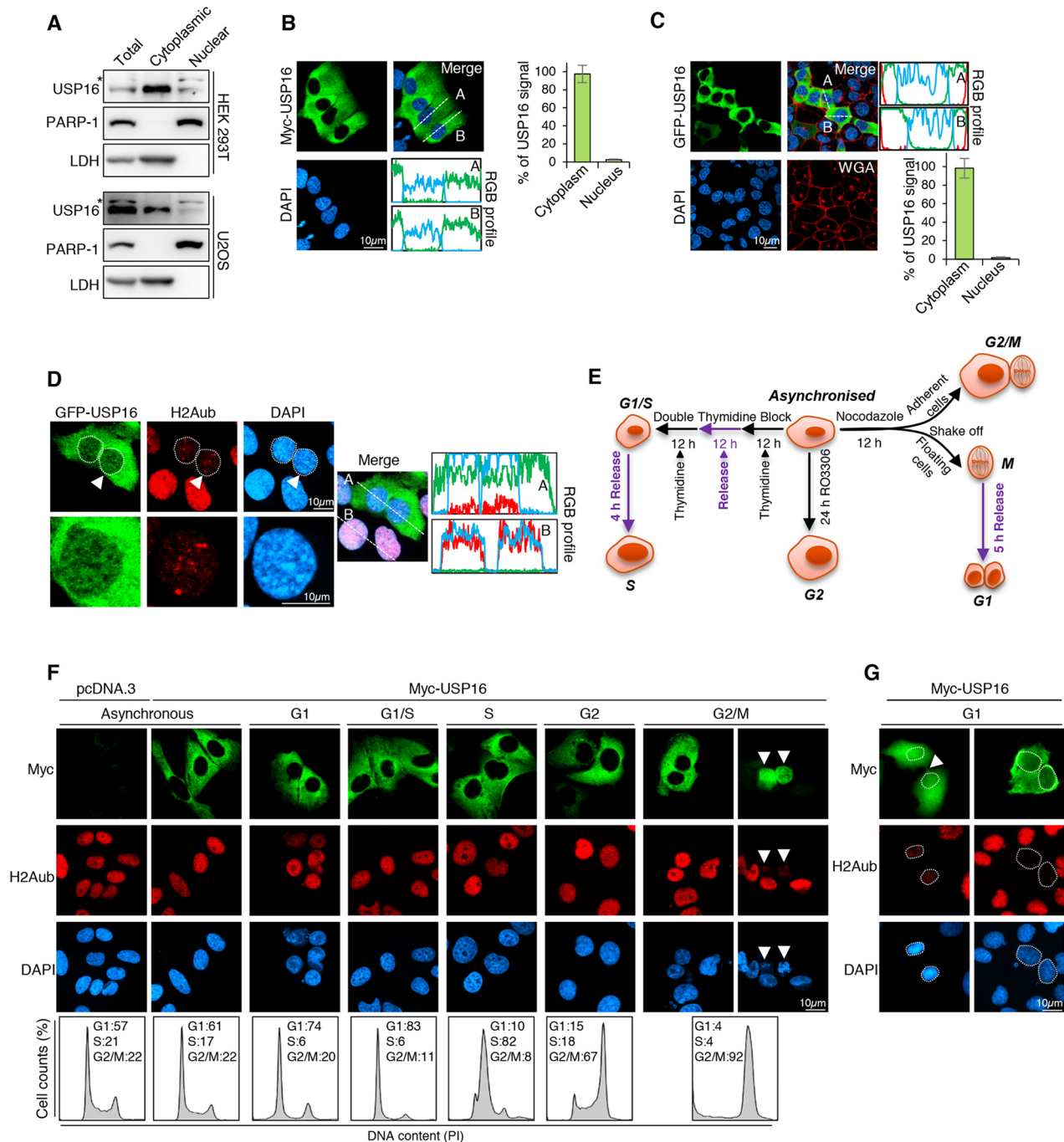


Fig. 1. USP16 is predominantly cytoplasmic during interphase. (A) Subcellular fractionation and analysis of USP16 protein levels. Nuclear and cytoplasmic fractions were analyzed by immunoblotting. The asterisk indicates an upper band, occasionally observed, that might correspond to a non-specific protein or a modified form of USP16. LDH and PARP-1 were used as controls for the cytoplasmic and nuclear fractions, respectively. Representative of $n=4$ biological replicates. (B) Determination of USP16 localization by immunostaining. U2OS cells stably expressing Myc-USP16 were used for paraformaldehyde fixation and immunofluorescence. RGB profiles for the indicated linescans for anti-Myc or DAPI staining were generated using ImageJ, and relative quantification of USP16 protein signal in the nucleus versus cytoplasm was conducted. Data are presented as the mean \pm s.d. percentage of USP16 signal in each compartment versus total signal and corresponds to an average quantification on 10 cells; $n=5$ biological replicates. (C) Determination of USP16 localization in live cells. U2OS cells stably expressing GFP-USP16 were used for the direct detection of GFP fluorescence. Alexa Fluor™ 594-conjugated wheat germ agglutinin (WGA) was used to stain plasma membrane. Relative quantification of USP16 protein was conducted as shown in B; $n=3$ biological replicates. (D) U2OS cells stably expressing GFP-USP16 were used for immunofluorescence analysis. The occasional presence of USP16 in nuclei is often observed in two adjacent cells. The nucleus highlighted with the arrowhead is shown magnified in the lower row. Relative intensity of USP16, H2Aub and DAPI signals was assessed; $n=3$ biological replicates. (E) Schematic representation of the procedures used to synchronize cells at different cell cycle phases. (F) U2OS cells were transfected with pcDNA.3 or GFP-USP16 constructs and following cell cycle synchronization (as indicated in E), subcellular localization of USP16 was determined. The cell cycle profile of each cell population was analyzed by propidium iodide staining and FACS (bottom panels). $n=3$ biological replicates. Arrowheads highlight cells with nuclear USP16. (G) The presence of USP16 in the nuclei of two adjacent cells is observed in G1 (1–3% of the total cell population). Two representative images are shown. The arrowhead indicates a cytoplasmic bridge between two daughter cells. Nuclei are encircled to indicate cells with nuclear USP16 and reduced levels of histone H2Aub. $n=3$ biological replicates.

never exceeds 1–3% of the G1 cell population. These results together show that USP16 is cytoplasmic in all cell cycle phases, but exhibits nuclear accumulation in a very small proportion of G1 cells.

USP16 is rapidly exported to the cytoplasm by the CRM1 system following M phase completion

It was previously observed that treatment of cells with leptomycin B (LMB), an inhibitor of CRM1 (also known as exportin 1)-mediated protein export, resulted in the accumulation of USP16 in the nucleus (Xu et al., 2013). However, (1) whether USP16 is actively imported into the nucleus through an NLS, (2) what are the kinetics and extent of USP16 entry into the nucleus, and (3) what are the molecular determinants responsible for USP16 nucleo-cytoplasmic transport, all remained unaddressed. Hence, we sought to rigorously study USP16 localization following inhibition of CRM1. Treatment of U2OS cells expressing Myc-USP16 with LMB caused an accumulation of this DUB in the nucleus with up to 35% of cells harboring both nuclear and cytoplasmic staining at 24 h post treatment (Fig. 2A,B). As control, the C2TA transcription factor, known to be regulated by nuclear export (Cressman et al., 2001), readily and rapidly accumulated in the nucleus in a majority of cells following 6 h of LMB treatment. We also observed that, upon accumulation of USP16 in the nucleus, histone H2Aub levels were considerably reduced. Of note, most CRM1-exported proteins accumulate relatively quickly (within few hours) in the nucleus following LMB treatment and often with a predominant nuclear localization (Cressman et al., 2001; Esmaili et al., 2010; Julien et al., 2003; Liu and DeFranco, 2000; Murai et al., 2003; Rodier et al., 2001). In contrast, we observed an unusually protracted accumulation of USP16 in the nucleus after LMB treatment. In addition, USP16 was either equally distributed between the cytoplasm and the nucleus, or remained predominantly cytoplasmic, following LMB treatment (Fig. 2A,B).

The observed nuclear localization of USP16 in G1 cells raised the possibility that USP16 might transiently reside in the nucleus after mitosis (Fig. 1G), which would explain the occasional presence of nuclear USP16 in two adjacent cells in early G1. If this is the case, blocking cell cycle progression through mitosis would be expected to reduce the number of cells containing USP16 in the nucleus. Accordingly, treatment with RO3366 results in a strong decrease in the proportion of cells with nuclear USP16 following LMB treatment (Fig. 2C,D). FACS analysis showed that RO3366 treatment results in nearly a 3-fold increase of G2 cells (Fig. 2C, bottom panels). We also observed an increase of histone H3S10 phosphorylation following CDK1 inhibition, confirming the accumulation of pre-mitotic cells (Figs 2C). Interestingly, when cells are released from RO3366 to enter mitosis, no distinct nuclear accumulation of USP16 could be observed (Fig. S2A). When chromosome condensation could be readily detected, USP16 was still observed in the cytoplasm (Fig. S2B). However, when chromosomes became clearly distinct (Fig. S2A, see 90 min time point), USP16 generally showed a homogenous cellular distribution, likely due to nuclear membrane breakdown. Overall, the above results suggest that USP16 does not enter the nucleus prior to the onset of mitosis. We also note that while phosphorylation of histone H3S10 is strongly increased at this stage, no deubiquitylation of H2Aub could be observed (Fig. S2C). Moreover, when considering the condition of LMB treatment alone, cells with nuclear USP16 always manifested low levels of histone H2Aub (Fig. 2C). However, no correlation could be made between the presence of USP16 in the nucleus and the levels of histone H3S10P. These results therefore indicate that H2Aub deubiquitylation is not a prerequisite for phosphorylation of H3S10.

To further determine whether USP16 transiently resides in the nucleus after mitosis, we synchronized cells in M phase with nocodazole followed by release into G1 in the presence or absence of LMB. FACS analysis confirmed the enrichment of G1 cells following mitotic exit (Fig. 2E). We observed that USP16 is retained in the nucleus following mitosis in the large majority of LMB-treated G1 cells (Fig. 2F,G). Nevertheless, USP16 was either evenly distributed between the cytoplasm and the nucleus or was primarily observed in the cytoplasm. Interestingly, this effect appeared to be specific to USP16, as two other cytoplasmic proteins, UBE2O and RPS6, are not retained in the nucleus following LMB treatment of nocodazole-released M phase cells (Fig. S2D,E). These results, taken together suggest that, during mitosis, USP16 is transiently retained in the nucleus following nuclear membrane breakdown and exported to the cytoplasm after nuclear membrane assembly. Alternatively, USP16 might be transiently imported and localized in the nucleus of early G1 cells. Under both scenarios, our data suggest that specific molecular determinants are responsible for transient retention of USP16 in the nucleus.

A non-canonical NLS moderately contributes to the nuclear localization of USP16

We sought to test the hypothesis that molecular determinants could be responsible for the transient nuclear localization of USP16. Using an NLS prediction algorithm (Nguyen Ba et al., 2009), we noticed several lysine/arginine-rich sequences that might act as nuclear targeting motifs (Fig. S3A). In particular, it has been reported that a lysine-rich region located within amino acids 124–197 could be responsible for USP16 nuclear localization (Xu et al., 2013). Within this region, amino acids 150–185 were identified by the NLS prediction algorithm, but with a low confidence score (Fig. S3A). We found that fusion of this sequence to the N-terminus of GFP [GFP^{150-185(USP16)}] resulted in a chimeric protein that did not actively accumulate in the nucleus when compared to GFP alone (Fig. S3B). GFP fused to the NLS sequence from SV40T large antigen [GFP^{NLS(TAg)}] and GFP alone were used as a positive and negative controls, respectively. Moreover, deletion of the 150–185 amino acid sequence in the context of the full-length protein (USP16^{Δ150-185}) had no impact on the localization of USP16 following treatment with LMB (Fig. S3C,D).

Two other lysine/arginine-rich stretches along USP16, namely, amino acids 1–9 (MGKKRRTKGGK) and 437–459 (KHLQKKAK-KQAKKQAKNQRQK), were also identified as potential nuclear-targeting sequences (Fig. S3A). The former sequence might act as a monopartite NLS, which usually comprises a small stretch of basic amino acid residues (Kosugi et al., 2009; Lange et al., 2007). The 437–459 amino acid region exhibited the highest probability score, but does not conform to either typical monopartite or bipartite NLS sequences, the latter being characterized by two small clusters of basic amino acids separated by 10 to 12 amino acids (Kosugi et al., 2009). Instead, the 437–459 region contains a stretch of lysine residues intercalated with multiple polar glutamine residues and is longer than a classical monopartite NLS. To determine the potential contribution of each of the two motifs to USP16 localization, we first fused each sequence to the C-terminus of GFP. Our results show that 437–459 amino acid region [GFP^{437-457(USP16)}], but not the 1–9 amino acid region [GFP^{1-9(USP16)}], is sufficient to target GFP to the nucleus (Fig. 3A). We therefore considered this sequence as the potential USP16 NLS [NLS^(USP16)]. This putative NLS resides between the first catalytic region and the linker domain, and is highly conserved from human to *Drosophila* (Fig. S3E).

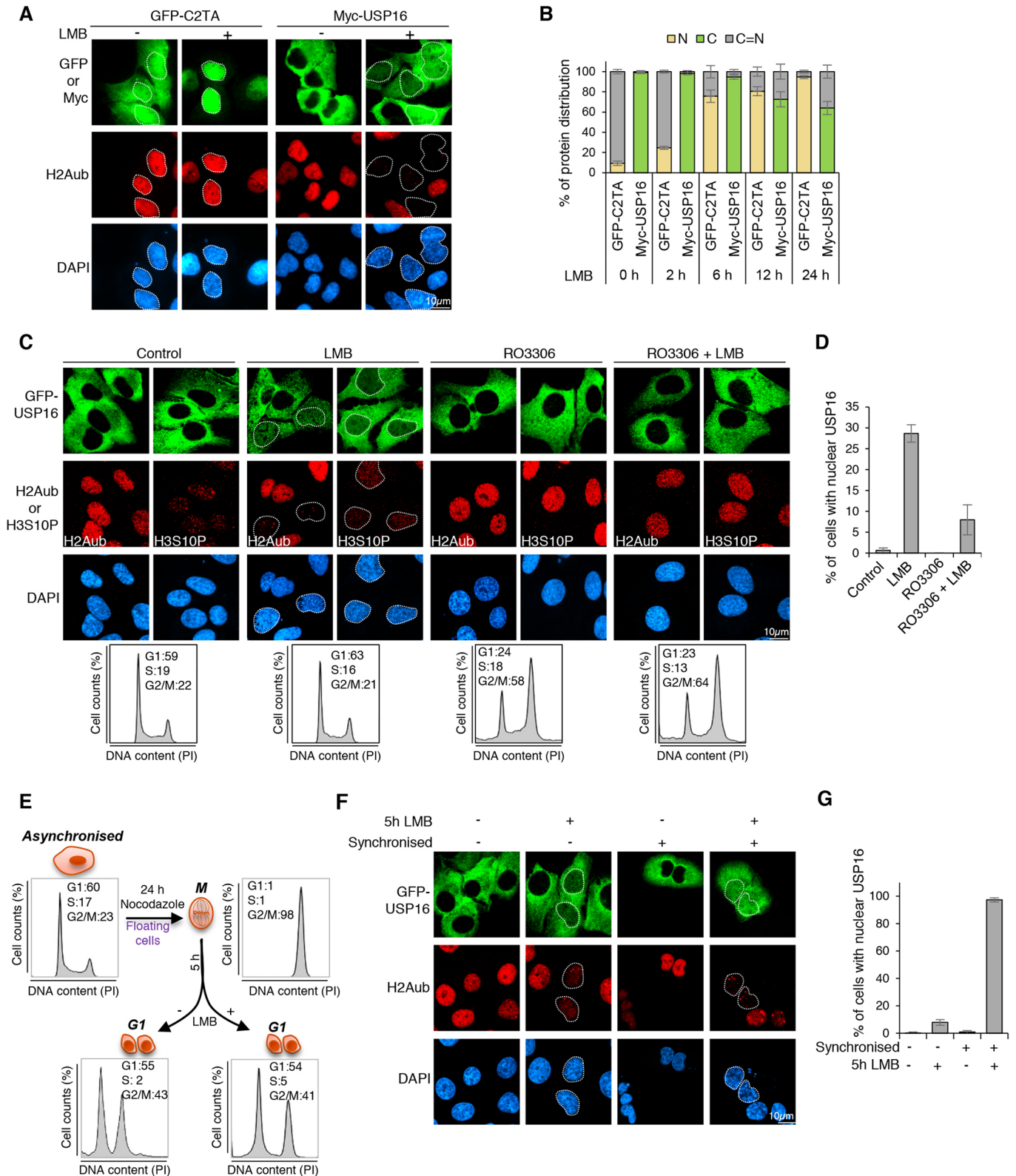


Fig. 2. See next page for legend.

We analyzed the importance of this potential NLS in the context of the full-length protein, and observed an ~2-fold reduction in nuclear accumulation of USP16^{NLS} following 24 h of LMB treatment, with ~17% of cells showing nuclear USP16 (Fig. 3B,C). Thus, the lysine rich 437–457 amino acid region of USP16 acts as

an NLS in its natural context. However, the USP16 NLS might not be completely exposed within its natural location in the context of the full-length protein. Indeed, when USP16 NLS is fused to the N-terminus of USP16 [USP16^{NLS(USP16)}], we observed a predominant cytoplasmic localization in untreated cells, whereas ~80% of cells

Fig. 2. USP16 is rapidly exported to the cytoplasm by a CRM1-mediated system following M phase completion. (A) USP16 localization following inhibition of CRM1. U2OS cells were transfected with pDEST Myc-USP16 WT or GFP-C2TA and treated with LMB for 24 h. The USP16 subcellular localization was then determined. The localization of GFP-C2TA was monitored as a positive control for LMB treatment. Representative of $n=3$ biological replicates. (B) Cell counts of USP16 nuclear localization was conducted (as in A). C, predominant in the cytoplasm; N, predominant in the nucleus, C=N, equal distribution between cytoplasm and nucleus. More than 100 cells were counted in three independent experiments and values are presented as mean \pm s.d. (C) Localization of USP16 following CDK1 inhibition. U2OS cells stably expressing GFP-USP16 were treated with RO3306 and/or LMB for 24 h. The USP16 subcellular localization and the levels of histone H2Aub and histone H3S10P were determined by direct GFP fluorescence or immunofluorescence. The cell populations were analyzed by FACS (bottom panels). $n=3$ biological replicates. (D) Cell counts for the nuclear localization of USP16 was conducted after RO3306 and/or LMB treatment (as shown in C). More than 100 cells were counted in three independent experiments and values are presented as mean \pm s.d. (E) Cell cycle profiles following release from mitotic block. U2OS cells stably expressing GFP-USP16 were blocked in metaphase following treatment with nocodazole. Partially adherent cells (mitotic population) were obtained by shake-off and released in the presence or absence of LMB for 5 h. Cell cycle profiles were determined by FACS analysis. (F) The USP16 subcellular localization and the levels of histone H2Aub were determined in cells treated as indicated in E and analyzed by direct fluorescence or immunofluorescence, respectively. (G) Cell counts for nuclear localization of USP16 was conducted after RO3306 and/or LMB treatment (as shown in E,F). More than 100 cells were counted in three independent experiments and values are presented as mean \pm s.d.

exhibited USP16 in both cytoplasm and nucleus following 24 h of LMB treatment (Fig. 3B,C). Nonetheless, this NLS remains less potent than the T antigen NLS, which led to the import of ~80% of USP16 [USP16^{NLS(TAg)}] into the nucleus after only 6 h of LMB treatment (Fig. 3B,C). Of note, as USP16 might form homotetramers *in vivo* (Joo et al., 2007), we wanted to test the possibility of endogenous USP16 self-interaction, which could impact the localization of USP16^{ANLS}. We used a combination of CRISPR/Cas9-mediated knockout with siRNA to increase the efficacy of USP16 protein depletion, as subsets of cells remain refractory to either approach (Fig. S4A,B). We did not observe noticeable differences in localization of Cas9/siRNA-resistant USP16^{WT} or USP16^{ANLS} between controls and the corresponding conditions following depletion of endogenous USP16 (Fig. S4C,D). Taken together, our data indicate that USP16 contains a functional NLS that partially contributes to its nuclear localization.

Catalytic dead USP16 remains trapped by PRC1 substrates in the nucleus

As the USP16 NLS is located between the two regions of the catalytic domain, we hypothesized that USP16 catalytic activity might impact its nucleocytoplasmic transport. To address this, we took advantage of our set-up whereby release from nocodazole in combination with LMB treatment results in a highly enriched cell population with nuclear USP16. FACS analysis confirmed the expected cell cycle profiles following mitotic exit (Fig. S4E). We found that mutating the catalytic cysteine residue to a serine residue (USP16^{C205S}) increased its nuclear retention, even in the absence of LMB (Fig. S4A,B). This was readily noticeable at 5 h post-release from mitotic block. It is interesting to note that USP16^{C205S} is either equally distributed between the nucleus and the cytoplasm, or even predominantly localized in the nucleus. However, the nuclear localization of this variant is not maintained after 24 h of release from mitotic block. Deletion of USP16 NLS (USP16^{ANLS-C205S}) only partially reduced nuclear localization of the catalytic dead mutant (Fig. 4A,B). These results suggest that USP16 catalytic

activity influences USP16 cytoplasmic localization after mitotic exit. However, since USP16^{C205S} is predicted not to lose its ability to bind ubiquitin, we reasoned that this mutant might remain tightly associated with H2Aub, which is highly abundant in the nucleus, thus underpinning the apparent nuclear localization of this mutant. Alternatively, self-deubiquitylation might also regulate USP16 localization, as we previously demonstrated for the DUB BAP1, whose nucleocytoplasmic localization is regulated by the E2 conjugating enzyme and E3 ligase hybrid denoted UBE2O (Mashtalir et al., 2014). To distinguish these possibilities, we first depleted Ring1A and Ring1B (also known as RNF1 and RNF2, respectively), the two major E3 ligases that act on H2A K119, and observed relocalization of USP16^{C205S} to the cytoplasm (Fig. 5A–C). To further demonstrate that ubiquitin binding is essential for USP16 nuclear localization, we modeled the structure of the catalytic domain for this DUB using the available crystal structures of USP2 and USP7, both in complex with ubiquitin, and inferred the amino acids necessary for ubiquitin binding by USP16 (Fig. 5D). The structural modeling of USP16 catalytic domain (the linker region between the CD1 and CD2 was removed) complies with the known features of the classical USP catalytic domain. Notably, we observed the three parts of a USP catalytic domain: the Fingers, Palm and Thumb. Importantly, the ubiquitin-binding pocket aligns very well with both the USP2 and USP7 ubiquitin-binding interfaces. Therefore, we generated two mutants within two portions of the catalytic domain, CD1-M or CD2-M. First, we validated, using two DUB activity probes, that a distinct upper band shift is observed for wild-type USP16, indicating that nearly all of the USP16 pool is labeled with the ubiquitin probe (Fig. 5E). In contrast, no band shift was observed for the CD1-M and CD2-M mutants indicating their inability to bind ubiquitin (Fig. 5E). Next, we transduced U2OS with wild-type USP16 and corresponding mutants, and found that ablation of ubiquitin binding completely prevents nuclear accumulation of USP16 (Fig. 5F,G). We conclude that catalytic inactive USP16 remains artificially trapped in the nucleus, that is, it cannot be released from PRC1 substrates and, notably, the highly abundant ubiquitylated H2AK119.

Mapping of domains regulating USP16 nucleocytoplasmic trafficking

We sought to identify the molecular determinants responsible for USP16 exclusion from the nucleus. First, we fused the T antigen NLS (NLS^{TAg}) to either the N- or C-terminus of USP16, and found that the resulting proteins, USP16^{NLS(TAg)-N} and USP16^{NLS(TAg)-C} are localized in the cytoplasm, but become predominantly or partially nuclear following LMB treatment, respectively. (Fig. S5A, B). Of note, fusing T antigen NLS to the N-terminus of USP16 promoted its nuclear entry more efficiently than the C-terminal fusion, suggesting that an additional molecular determinant at the C-terminus of USP16 is involved in coordinating its nuclear localization. However, the T antigen NLS might not be similarly exposed when fused to N-terminus versus C-terminus of USP16. Thus, GFP was fused between T antigen NLS and USP16 at both N- and C-termini. Interestingly, the effect of T antigen NLS is still more important when fused to USP16 N-terminus (Fig. S5A,B). This suggests that a free C-terminus of USP16 might be involved in coordinating its subcellular localization. Nonetheless, in all cases, USP16 is excluded from the nucleus, and its nuclear accumulation is observed only after LMB treatment. Notably, a previous study suggested that the sequence near leucine 685 at the C-terminus of USP16, within the second region of the catalytic domain, might act as a CRM1-dependent NES (Xu et al., 2013) (Fig. S5C). When we

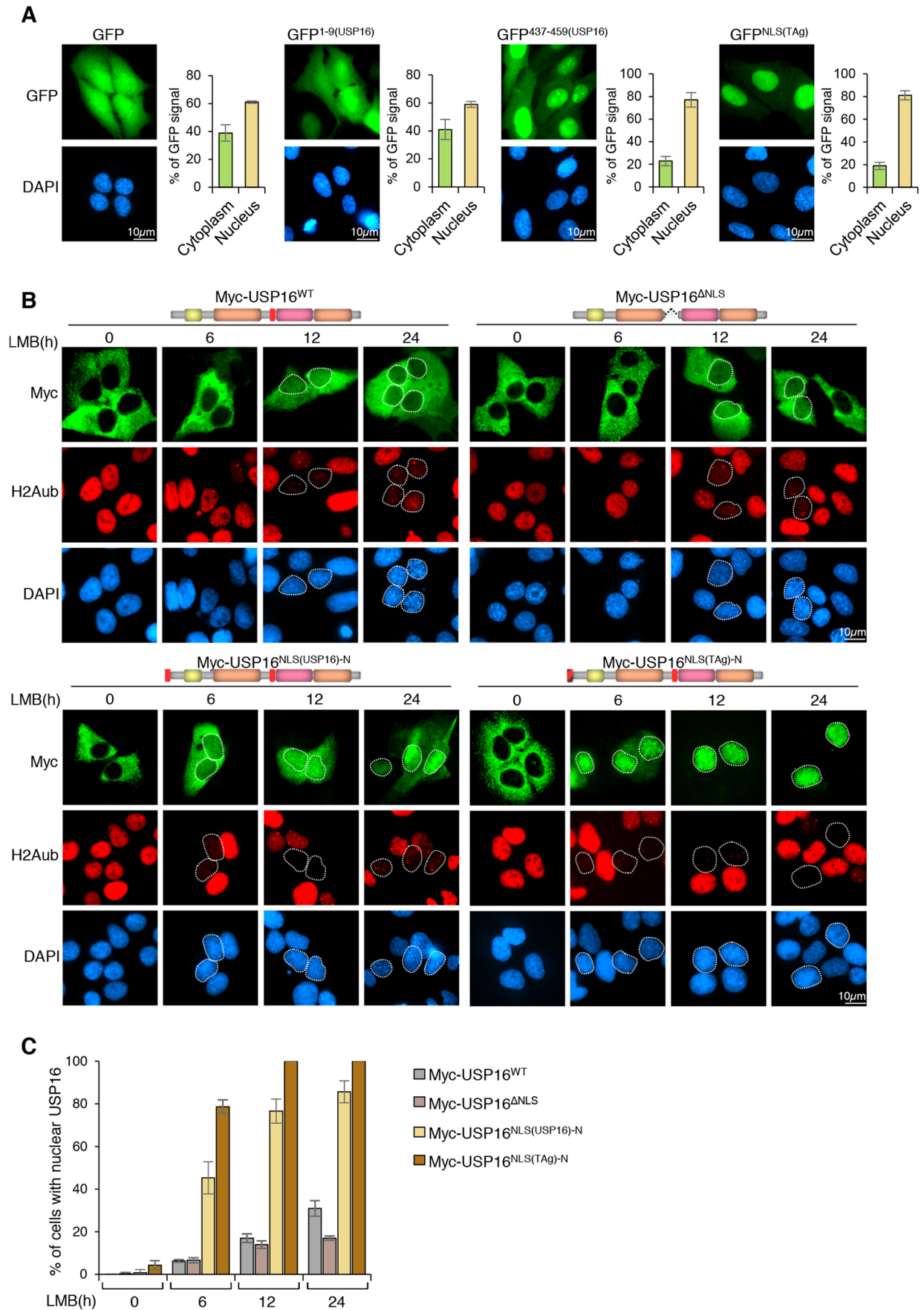


Fig. 3. See next page for legend.

Fig. 3. Identification of a nuclear localization signal of USP16.

(A) Examination of several potential NLS sequences of USP16 for targeting GFP into the nucleus. U2OS cells were transfected with pOD35 GFP, pOD35 GFP 1-9 (USP16), pOD35 GFP 437-459 (USP16) or pOD35 GFP NLS (TAG) expression constructs. The subcellular localization of the GFP fusion proteins was detected by fluorescence microscopy. Quantification of GFP signal in the nucleus versus cytoplasm was conducted. Data is presented as the mean \pm s.d. percentage of GFP signal in each compartment versus total signal and corresponds to an average quantification on 10 cells; $n=5$ biological replicates. (B) Evidence for a functional USP16 NLS. U2OS stably expressing Myc-USP16^{WT}, Myc-USP16 ^{Δ NLS}, Myc-USP16^{NLS(USP16)-N} or Myc-USP16^{NLS(TAG)-N} were treated with LMB and used for immunofluorescence analysis. Schematic representation of the different USP16 mutants are shown at the top of each panel. (C) Cell counts from experiments performed as indicated in B represent the percentage of cells with nuclear USP16. More than 100 cells were counted and the values are presented as mean \pm s.d.; $n=3$ biological replicates.

fused this peptide sequence to the N-terminus of GFP [GFP⁶⁸⁵⁻⁷⁰⁸ (USP16)], we did not observe exclusion of the chimeric protein from the nucleus (Fig. S5D). In addition, deletion of this sequence from USP16 (USP16 ^{Δ 685-708}) does not perturb its retention in the cytoplasm nor its accumulation in the nucleus following LMB treatment (Fig. S5E,F). We also tested other leucine-rich regions of USP16 (301-313 and 374-392 amino acid sequences) as GFP fusions, and observed no effect on GFP localization (Fig. S5C,D). The NES from the HIV-1 REV protein was included as a positive control, which significantly excluded GFP from the nucleus to the cytoplasm. We then generated several deletion mutants of USP16 and tested their localization with and without LMB treatment. Deletion of either the C- or N- terminus of USP16, USP16 ^{Δ C-term} or USP16 ^{Δ N-term}, respectively, did not have a major effect on USP16 localization in untreated cells (Fig. 6A,B). However, treatment with LMB resulted in nuclear retention of USP16 ^{Δ N-term}, but not USP16 ^{Δ C-term}. Next, we deleted each of the two regions of the catalytic domain (CD1 and CD2) without removing the linker region and observed that, while deletion of CD1 did not impact USP16 localization, deletion of CD2 strongly reduced USP16 nuclear retention following LMB treatment (Fig. 6A,B). These results further support our initial observations that a molecular determinant promoting USP16 nuclear localization is located in the C-terminal region. Importantly, in the absence of LMB treatment, we found that only the deletion of the linker region (460-618 amino acid sequence) resulted in partial nuclear retention of USP16. About 40% of cells showed USP16 either evenly distributed between the cytoplasm and nucleus or mostly localized in the cytoplasm, but with a distinct nuclear signal, and this was associated with a strong reduction of H2Aub levels (Fig. 6A,B). Moreover, no major change was observed in the localization of USP16 ^{Δ linker} upon LMB treatment. Interestingly this linker region separates the USP16 catalytic domain into two regions (amino acids 191-402 and 617-777) and its deletion does not impact DUB activity. Mutation of the catalytic cysteine residue resulted in increased nuclear localization of USP16 lacking the linker region USP16 ^{Δ linker-C205S}. By contrast, unlike for wild-type USP16 (Fig. S5A,B), addition of TAG-NLS to the N-terminus of USP16 lacking the linker domain [USP16 ^{Δ linker-NLS(TAG)-N}] caused dramatic nuclear accumulation of this DUB, and this correlated with an increased proportion of cells with reduced levels of H2Aub (Fig. 6A,B). Next, we transduced U2OS cells with lentiviral vectors for USP16 expression with or without the linker region (USP16 ^{Δ linker}) and conducted fractionation of nuclear and cytoplasmic proteins. This confirmed that a substantial fraction of USP16 ^{Δ linker-C205S} remained associated with the nucleus compared to the fraction for the cytoplasmic

enzyme LDH (Fig. 6C). We conclude that the linker sequence between the two regions of the catalytic domain must contain a determinant that ensures the cytoplasmic localization of USP16.

Identification of the authentic NES in USP16

We sought to further characterize the USP16 linker domain (amino acids 460-618) (Fig. 7A), and found that this sequence was sufficient to retain GFP fusion protein in the cytoplasm, and to confer LMB responsiveness (Fig. 7B,C). A similar result was obtained when we incorporated the TAG-NLS into the GFP-Linker construct [GFP-Linker^{NLS(TAG)-N}] (Fig. 7B,C). These data suggest that the linker region of USP16 contains an NES that is sufficient to exclude USP16 from the nucleus. Therefore, we divided the linker into multiple overlapping amino acid sequences (Fig. 7A). Remarkably the P2 and P5 fragments, which share a common sequence, were able to retain GFP in the cytoplasm as demonstrated by nuclear accumulation upon LMB treatment (Fig. 7B,C). We further divided the P5 fragment into regions, P6, P7 and P8, and found that P6 was mostly in the cytoplasm and is responsive to LMB (Fig. 7B,C). Indeed, comparing P6 to other known NES sequences revealed a hydrophobic (Φ) residue-rich region (ISNGFKNLNL) that is different from the previously proposed USP16 export motif (Xu et al., 2013), but fulfills the criteria that define a NES motif [Φ -X-(2,3)- Φ -X(2,3)- Φ -X- Φ ; Fu et al., 2011; Fung et al., 2017]. This region of USP16 is highly conserved through evolution (Fig. S6A) and aligns with other known NES sequences (Fig. S6B). Next, we used the identified USP16 NES sequence to conduct molecular modeling, using a known crystal structure of PKI NES bound to the CRM1-Ran-RanBP1 complex and found that the identified USP16 NES matches the CRM1 NES-binding pocket (Fig. 7D). Finally, we generated a U2OS cell line stably expressing a USP16 construct lacking the export motif (USP16 ^{Δ NES}) and validated that USP16 accumulates in the nucleus without LMB treatment (Fig. 7E,F). We also depleted endogenous USP16 using a combination of CRISPR/Cas9 and siRNA, and did not observe changes in the localization USP16 ^{Δ NES} with or without LMB treatment (Fig. S6C,D). Finally, we tested the interaction of the USP16 linker or its NES, and observed a strong interaction with CRM1 *in vitro* (Fig. S6E). We conclude that USP16 is maintained in the cytoplasm due to the presence of a potent NES located between the two regions of the catalytic domain.

USP16 is not imported in the nucleus during genotoxic stress, but its enforced nuclear localization inhibits the assembly of DNA repair foci

Following induction of DNA double-strand breaks (DSBs), several proteins are rapidly recruited to DNA damage sites to form repair foci including phosphorylated H2AX (γ H2AX), as well as 53BP1 and BRCA1, two factors that promote DSB repair via non-homologous end joining (NHEJ) and homologous recombination (HR), respectively (Panier and Boulton, 2014; Zimmermann and de Lange, 2014). A previous finding showed that both overexpression and knockdown of USP16 perturbs DSB repair (Zhang et al., 2014), although a recent study reported that USP16 overexpression does not impact DSB repair foci (Wang et al., 2016). Thus, it remained unclear whether and, eventually, how USP16 could directly impact DSB repair. These conflicting results prompted us to determine whether USP16 undergoes translocation to the nucleus to directly regulate histone ubiquitylation during DNA damage repair. However, we did not observe any detectable accumulation of USP16 in the nucleus following ionizing radiation (IR) treatment of U2OS or IMR90 lung fibroblasts (Fig. S7A,B). Moreover, we

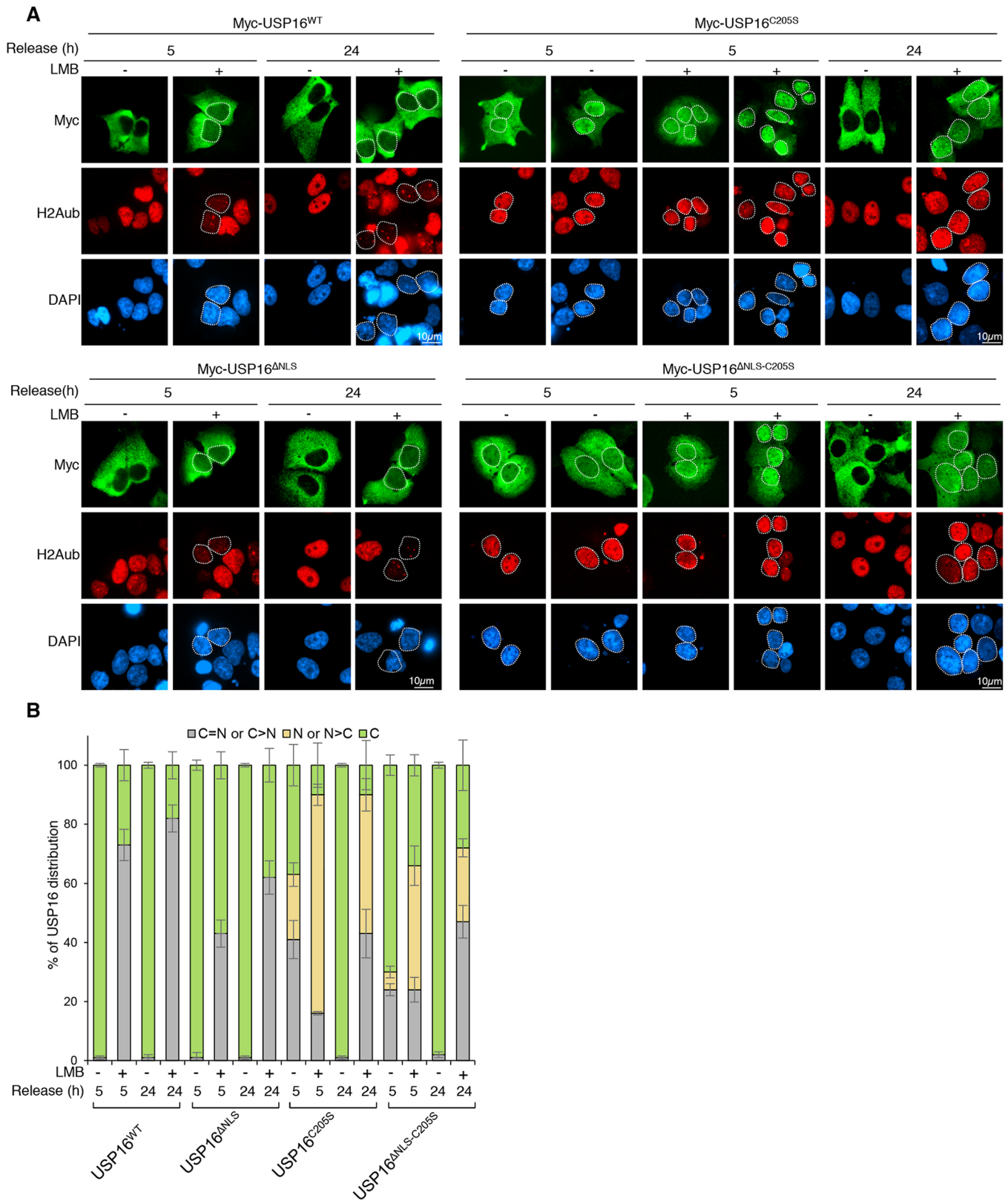


Fig. 4. Inhibition of DUB activity results in USP16 cytoplasmic localization. (A) Mutation of the catalytic cysteine residue results in USP16 nuclear retention. U2OS stably expressing Myc-USP16^{WT} and its catalytically inactive mutant Myc-USP16^{C205S}, or Myc-USP16^{ANLS} or Myc-USP16^{ANLS-C205S} were treated with nocodazole for 24 h. Mitotic cells were harvested by shake-off and then released for 5 h or 24 h in the presence or absence of LMB. The subcellular localization of USP16 was detected by immunofluorescence. (B) Cell counts from experiments shown in A representing the percentage of cells with nuclear and/or cytoplasmic USP16. N, predominantly nuclear; N>C, mainly in the nucleus rather than the cytoplasm; C=N, equal distribution between cytoplasm and nucleus; C>N, mainly in the cytoplasm rather than the nucleus; C, predominantly cytoplasmic. More than 100 cells were counted in three independent experiments and values are presented as mean±s.d.; n=3 biological replicates.

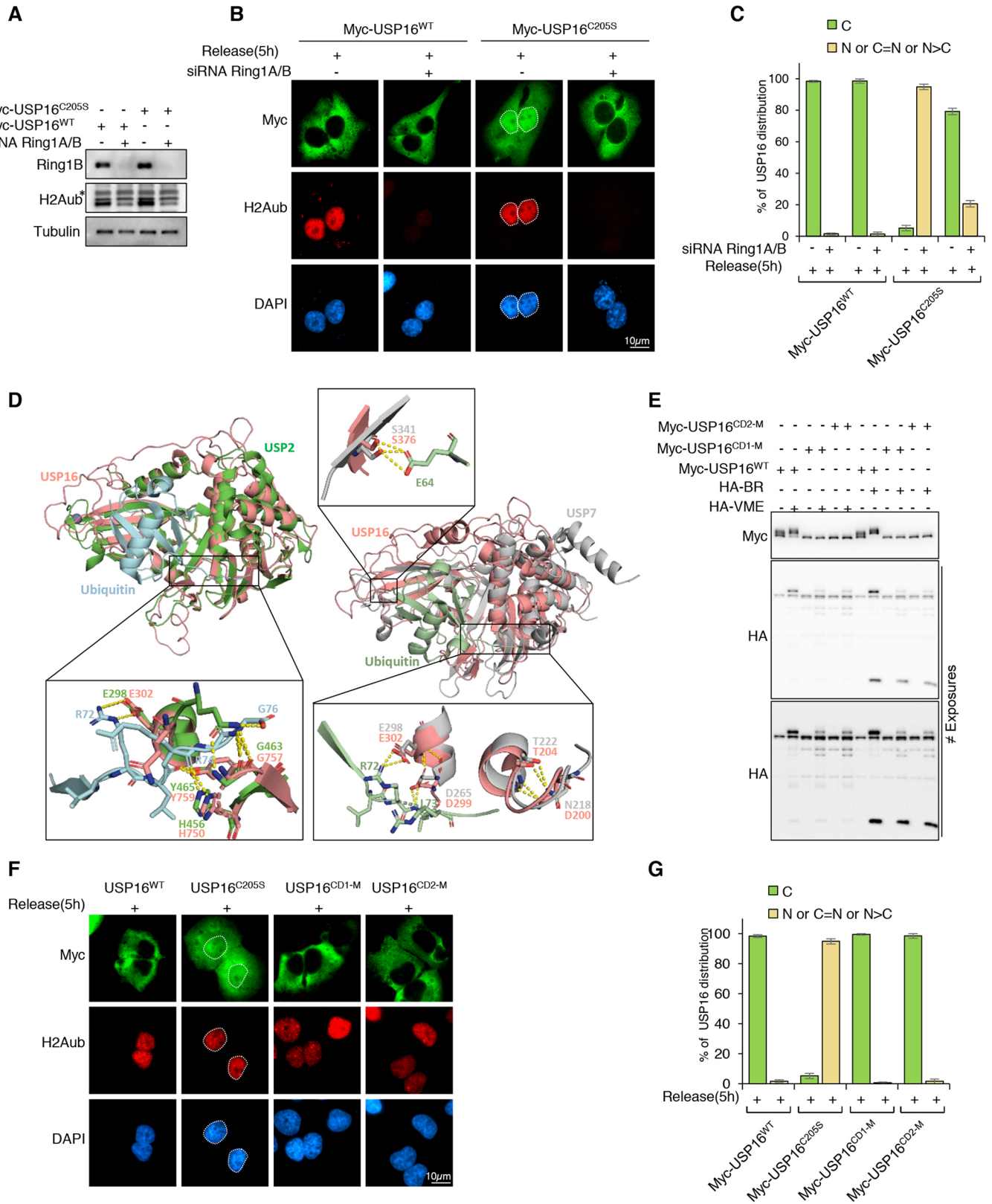


Fig. 5. See next page for legend.

conducted cell fractionation of U2OS stably expressing Myc-USP16, and again did not observe any increase in nuclear USP16 post IR (Fig. S7C). Next, we expressed USP16 and its mutants (USP16^{C205S}, USP16^{Δlinker} and USP16^{Δlinker-C205S}) to determine

their impact on DNA repair foci. U2OS cells were treated or not for 24 h with LMB, exposed to IR and then analyzed 4 h later. In the absence of IR, no spontaneous 53BP1 foci were observed following USP16 transfection, even when this DUB localizes to the nucleus

Fig. 5. Catalytic dead USP16 remains trapped by Ring1A and Ring1B substrates. (A) U2OS stably expressing Myc-USP16^{WT} or Myc-USP16^{C205S} were transfected twice with control (NT) or Ring1A and Ring1B siRNAs for 72 h and used for immunoblotting. Tubulin was a loading control. The asterisk indicates a non-specific band. Representative of *n*=3 biological replicates. (B) U2OS stably expressing Myc-USP16^{WT} or Myc-USP16^{C205S} were transfected twice with control (NT) or Ring1A and Ring1B siRNAs and treated with nocodazole for 24 h. Mitotic cells were isolated by shake-off, released for 5 h and then used for immunostaining. (C) Cell counts from the experiment shown in B representing the percentage of cells with nuclear and/or cytoplasmic USP16. N, predominantly nuclear; N>C, mainly in the nucleus; C=N, equal distribution between cytoplasm and nucleus; C, predominantly cytoplasmic. More than 100 cells were counted in three independent experiments and values are presented as mean±s.d.; *n*=3 biological replicates. (D) Overall view of the structural modeling of USP16 catalytic domain. The structure resembles catalytic core domain of USP7/HAUSP. Structural alignment of USP16 with USP2 (left panel) and with USP7 (right panel) catalytic domains are presented. Both models show the alignment of USP16 catalytic domain for ubiquitin binding. Hydrogen bonds between the C-terminus of ubiquitin and USP16 residues are shown by the yellow dashes in the magnified image of the USP16–ubiquitin binding interface. USP16 catalytic domain (CD) is in salmon, USP2 CD in green, USP7 CD in gray, ubiquitin in aquamarine (left panel) or green (right panel). (E) Lysates from cells stably expressing USP16^{CD1-M} or USP16^{CD2-M} were labeled with HA-tagged ubiquitin-VME or ubiquitin-Br DUB activity probes and analyzed by immunoblotting. *n*=2 biological replicates. (F) U2OS stably expressing Myc-USP16^{WT}, Myc-USP16^{C205S} or its ubiquitin-binding mutant forms Myc-USP16^{CD1-M} and Myc-USP16^{CD2-M} were treated with nocodazole and mitotic cells were harvested and released for 5 h before immunostaining. Representative of *n*=3 biological replicates. (G) Cell counts from experiments shown in D representing the percentage of cells with nuclear and/or cytoplasmic USP16. N, predominantly nuclear; N>C, mainly in the nucleus rather than the cytoplasm; C=N, equal distribution between cytoplasm and nucleus; C, predominantly cytoplasmic. More than 100 cells were analyzed and values are presented as mean±s.d.; *n*=3 biological replicates.

following either LMB treatment or deletion of the linker domain (Fig. 8A,B). Strikingly, the presence of USP16^{Δlinker} in the nucleus post IR was associated with a strong decrease in 53BP1 foci formation, which was dependent on the catalytic activity of USP16 (Fig. 8A,B). Upon LMB treatment, USP16 nuclear retention also prevented IR-induced foci formation in a DUB activity-dependent manner (Fig. 8A,B). Under all conditions, treatment with IR did not induce noticeable changes in the localization of USP16 or its mutants (Fig. 8C). Taken together these results suggest that unscheduled accumulation of USP16 in the nucleus abrogates DSB repair.

DISCUSSION

In this study, we provide novel insight into the function of USP16, and clarify the mechanisms that coordinate its trafficking between the cytoplasm and nucleus. First, our data indicate that USP16 is essentially cytoplasmic in all phases of the cell cycle including late G2, and is retained transiently in the nucleus during a brief period post mitosis. We identified a strong NES signal within the linker domain, which constitutes the major determinant of USP16 cytoplasmic localization. Moreover the hydrophobic amino acids that define the functionality of this motif, and which are critical for NES interaction with CRM1, are invariably found in most vertebrates, suggesting the biological importance of USP16 nuclear export. Second, we found that a catalytic dead USP16 mutant is retained in the nucleus through its ability to bind ubiquitylated proteins. Third, USP16 contains a functional, but weak, NLS that operates, in the context of the full-length protein, to influence USP16 subcellular localization. Fourth, while depletion of USP16 results in a DNA repair delay, this DUB is

not actively translocated into the nucleus in response to genotoxic stress. Instead, only enforced expression of USP16 lacking its nuclear export signal inhibits DNA repair. Finally, we found that USP16 depletion results in the accumulation of conjugated ubiquitin species, likely reflecting a global perturbation of ubiquitin pools. This would be consistent with the presence of a ZNF UBP domain in USP16, which is known to bind the C-terminal di-glycine motif of unconjugated ubiquitin (Reyes-Turcu et al., 2006).

Cell fractionation experiments showed that a small pool of USP16 remains associated with nuclei even following their purification on a sucrose cushion. We initially hypothesized that this pool of USP16 is in the nucleus and might correspond to a subpopulation of cells at a specific phase of the cell cycle or that a small portion of USP16 could be uniformly present in the nucleus across all cell populations. Immunostaining studies indicated that only background signals could be observed in the nucleus for the majority of cells, arguing against USP16 nuclear localization in interphase. Moreover, it is unlikely that the pool of USP16 that co-fractionates with nuclei corresponds to the early G1 cells with nuclear USP16, as the proportion of the cells is extremely low within an unsynchronized cell population. Instead, this pool of USP16 might be associated with the fraction of organelles that inherently co-sediments with nuclei. Thus, while we cannot definitely exclude the presence of minute levels of USP16 in the nucleus that are below the detection limit, our results suggest that the main roles of USP16 are exerted within the cytoplasm during interphase. As such, it would be interesting to further determine the subcellular distribution of USP16 within the cytoplasm, as well, as the precise function of USP16 in this compartment.

We provided evidence indicating that, under normal growth conditions, USP16 nuclear import does not occur before M phase. First, cell cycle arrest at the G2/M border following CDK1 inhibition is not accompanied by an enrichment in the percentage of cells with nuclear USP16. By contrast, a strong reduction of nuclear USP16, which is otherwise promoted by LMB treatment, could be observed following CDK1 inhibition. Importantly, even after cell cycle release from CDK1 inhibition, no enrichment of USP16 in the nucleus was apparent prior to the onset of mitosis. This result is in contrast with previous findings suggesting that phosphorylation of USP16 by CDK1 inhibits its export and promotes its nuclear localization (Xu et al., 2013). On the other hand, we also found that, in the absence of LMB treatment, no global deubiquitylation of H2AK119 could be detected in CDK1-inhibited G2 cells, while a strong increase of histone H3S10 phosphorylation was observed. Thus, H3S10 phosphorylation precedes mitotic H2Aub deubiquitylation, in contrast to previous results reporting the reverse relationship (Joo et al., 2007). Our results also argue against a direct role of USP16 in chromosome condensation, but whether there is a relationship between phosphorylation of histone H3S10 and subsequent deubiquitylation of histone H2Aub will require further investigation.

We established that USP16 resides in the nucleus for only a very short period of time after mitosis. This conclusion is based on several observations: (1) in an asynchronous cell population, only a very small proportion of cells (less than 1%) could be captured with nuclear USP16; (2) only after LMB treatment in combination of mitotic block release could nuclear USP16 be observed in a heterogeneous population of cells; (3) when USP16 is observed in the nucleus, this often corresponds to two adjacent cells, likely corresponding to daughter cells; and (4) USP16 nuclear localization partially depends on its atypical, but functional, NLS. The function

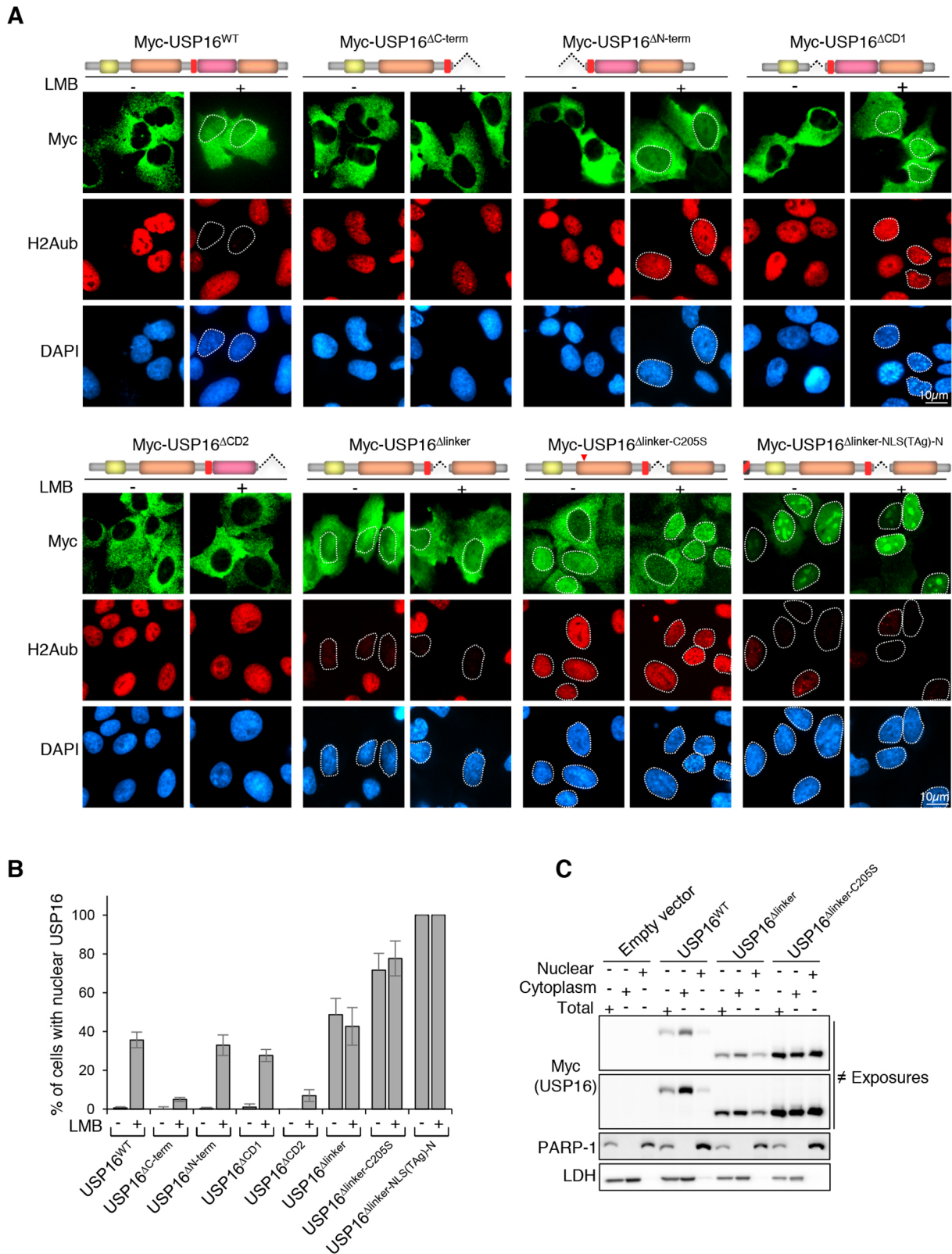


Fig. 6. The linker region within the catalytic domain is responsible for USP16 cytoplasmic retention. (A) Mapping of USP16 domains responsible for its nuclear export. U2OS cells were transduced with lentiviruses to express various mutants of USP16. Cells were then treated with LMB for 24 h, and the subcellular localization of USP16 mutants was determined by immunofluorescence. Schematic views of the mutants are presented at the top of each panel. Representative of $n=3$ biological replicates. (B) Cell counts from experiments shown in A representing the percentage of cells with nuclear USP16. For each condition, more than 100 cells were counted and values are presented as mean \pm s.d.; $n=4$ biological replicates. (C) The linker domain is responsible for USP16 cytoplasmic localization. U2OS cells stably expressing empty vector, Myc-USP16^{WT}, Myc-USP16^{Δlinker} or Myc-USP16^{Δlinker-C205S} were harvested, and the nuclear and cytoplasmic fractions were obtained by fractionation and used for immunoblotting. LDH and PARP-1 were used as loading control for the cytoplasmic and nuclear fractions, respectively. Representative of $n=3$ biological replicates.

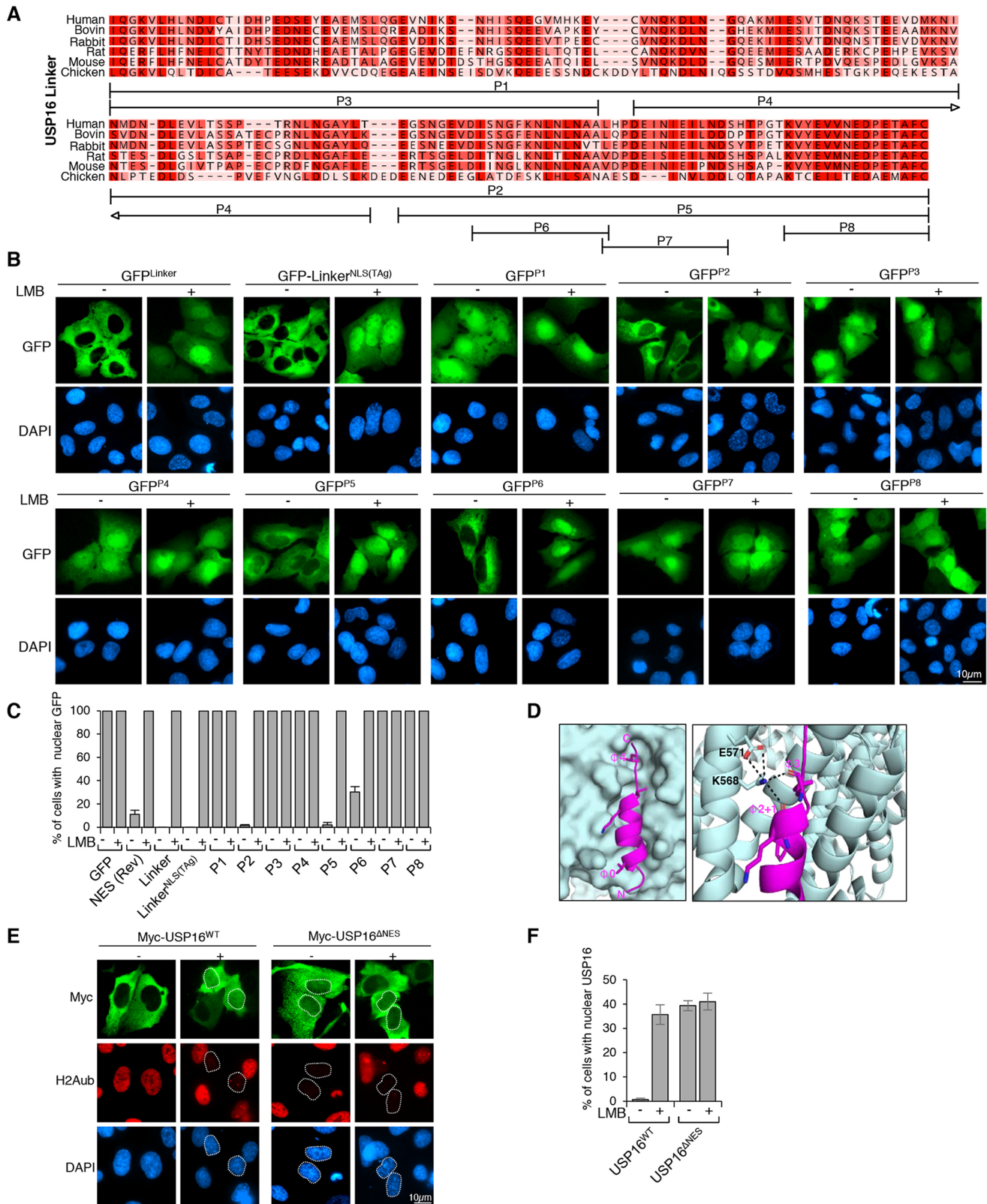


Fig. 7. See next page for legend.

of USP16 in the nucleus in early G1 remains unknown, but could be required for post-mitotic deubiquitylation of residual H2Aub. Alternatively, a yet-to-be-discovered function of USP16 could take place in early G1 cells during chromosome decondensation and

chromatin reorganization. Of note, the NLS of USP16, although lysine rich, is quite unusual and does not correspond to previously known nuclear import sequences (Lange et al., 2007; Soniat and Chook, 2015).

Fig. 7. Identification of the USP16 NES. (A) Sequence conservation of the linker region of USP16. Sequences were obtained from UniProt and aligned using Geneious R8. A representation of the various regions of USP16 linker (P1 to P8) fused to the N-terminus of GFP as used in this study are shown underneath. (B) The USP16 NES is sufficient to retain GFP in the cytoplasm. U2OS cells were transfected with either pEGFP N3, GFP NES (HIV1 REV), GFP-linker, GFP-linker-NLS (T Large Antigen) or the various GFP fusion constructs shown in A (P1 to P8). Cells were treated with LMB for 24 h and the subcellular localization of these GFP fusions was determined. (C) Cell counts from experiments performed as indicated in B showing nuclear localization of GFP fusions in transfected cells before and after LMB treatment. For each condition, more than 100 cells were counted and values are presented as mean±s.d.; $n=3$ biological replicates. (D) Cartoon representation of the homology model of USP16 NES in complex with CRM1. The left panel shows the NES binding to the CRM1 groove. The $\Phi 0$ and $\Phi 4$ amino acids represent the start and the end of the NES consensus. Side chain representation of amino acids is shown. The right panel shows the amino acids that make contacts between USP16 NES ($\Phi 2+1$ and $\Phi 3$) and CRM1 groove (K568 and E571). The hydrogen bonds are shown by the black dashes. Φ denotes hydrophobic amino acid. (E) U2OS stably expressing Myc-USP16^{WT} or Myc-USP16^{ΔNES} were treated with LMB for 24 h. The subcellular localization was determined by immunofluorescence. Representative of $n=3$ biological replicates. (F) Cell counts from experiments performed as shown in E indicating nuclear localization of USP16. For each condition, more than 100 cells were counted and values are presented as mean±s.d.; $n=3$ biological replicates.

We also found that abolition of USP16 catalytic activity leads to enhanced nuclear retention of USP16 in G1 cells. This effect is only partially reduced following deletion of the USP16 NLS. Our data strongly suggest that catalytic dead USP16 remains strongly bound to ubiquitylated nuclear proteins through its catalytic domain, preventing its release and export to the cytoplasm. Consistent with this, deletions or mutations of the catalytic domain (CD1 or CD2), which would be expected to destroy the ubiquitin-binding interface of USP16, did not result in increased nuclear accumulation of USP16. Finally, depletion of Ring1A and Ring1B E3 ligase of H2AK119 strongly reduced nuclear localization of the catalytic dead USP16 mutant. Whether changes in the localization of catalytically inactive USP16 might reflect a physiological regulation remains to be investigated. In addition, it will be interesting to determine whether disease-associated mutations inactivate USP16 without altering its ability to bind ubiquitin, which in turn might have potential deleterious effects on H2Aub functions.

Our studies raise an important question regarding the roles of USP16 in the cytoplasm versus the nucleus. Since USP16 is predominantly cytoplasmic and, only following mitosis is rapidly exported to the nucleus where it remains for only a brief period, the function of USP16 NES appears to predominate over that of its NLS. Even when fused to the T antigen NLS, USP16 remains predominantly localized in the cytoplasm. These results suggest that USP16 activity might be deleterious in the nucleus under normal conditions, except at the end of mitosis, when this DUB might be needed to complete deubiquitylation of H2Aub before its exit to the cytoplasm. It is possible that USP16 is a promiscuous DUB that must be actively excluded from the nucleus to prevent undesirable deubiquitylation of nuclear proteins, events that can profoundly impact DNA repair mechanisms and epigenetic information. Of note, inhibition of USP16 export by LMB or deletion of its NES results in nuclear retention of this DUB in only a third of the total cell population, although these cells still do not show a predominant nuclear accumulation. Thus, we postulate that USP16, which resides in the cytoplasm during almost the entire cell cycle, might exert heretofore unknown critical functions in this compartment. Another interesting point regards the phylogenetic co-evolution of NLS and

NES sequences of USP16. It seems that the NLS appeared before the NES (Figs S3E, S6A), suggesting that USP16 might have preserved an ancestral function in the nucleus, and that its nuclear export with the potential acquisition of important cytoplasmic functions appeared later during evolution. Clearly, our study highlights the need of investigating the potential activity of this DUB in the cytoplasm and how its enzymatic activity is regulated to prevent potential promiscuous deubiquitylation.

MATERIALS AND METHODS

Antibodies

Mouse monoclonal Anti-Flag (M2) (cat. #F3165) and anti-Myc (cat. #9E10) antibodies were obtained from Sigma-Aldrich and Covance, respectively. A rabbit polyclonal anti-USP16 antibody was generated in-house using a bacteria-purified N-terminal fragment of the human protein (service provided by EZ Biolabs). Rabbit monoclonal anti-H2Aub (D27C4) (cat. #8240) was obtained from Cell Signaling Technology. Mouse monoclonal anti-RPS6 (C8) (cat. #sc-74459), mouse monoclonal anti- α -Tubulin (B-5-1-2) (cat. #sc-23948), mouse monoclonal anti-LDH (H-10) (cat. #133123), mouse monoclonal anti-PARP-1 (F-2) (cat. #sc-8007), mouse monoclonal anti-BRCA1 (D-9) (cat. #sc-6954), mouse monoclonal anti-Ring1B (N-32) (cat. #sc-101109), mouse monoclonal anti-ubiquitin (P4D1) (cat. #sc-8017), rabbit polyclonal anti-YY1 (H414) (cat. #sc-1703) and rabbit polyclonal anti-53BP1 (H300) (cat. #sc-22760) were purchased from Santa Cruz Biotechnology. Rabbit polyclonal anti-USP16 (cat. #14055-1-AP) was obtained from Proteintech. Mouse monoclonal anti-phospho-H3 (Ser10) (3H10) (cat. #05-806), mouse monoclonal anti-phospho-H2AX (Ser139) (JBW301) (cat. #05-636) and rabbit polyclonal anti-phospho-H3 (Ser10) (cat. #06-570) were obtained from Millipore. Rabbit polyclonal anti-USP16 (cat. #ab189838) was purchased from Abcam. Mouse monoclonal anti-HA hybridoma supernatant was used as previously described (Mashtalir et al., 2014). Additional information is described in Table S1.

Molecular cloning and plasmids

siRNA-resistant human USP16 was generated by gene synthesis (BioBasic) and subcloned into pENTR D-Topo (Life Technologies), to generate pENTR USP16. All USP16 cDNA sequences were manually modified using codon degeneracy (Table S2). The USP16 C205S construct was generated by DNA synthesis of a fragment containing a mutation in pBluescript plasmid (Biobasic) and then subcloned into the pENTR D-Topo plasmid containing USP16. The mutant cDNA constructs USP16 Δ NLS, USP16 Δ 150-185, USP16 Δ 685-708, USP16 Δ Linker, USP16 Δ Linker-C205S, USP16 Δ NLS-C205S, USP16 NLS (Tag)-N, USP16 NLS (Tag)-C, USP16 NLS (USP16)-N, USP16-GFP NLS (Tag)-C, GFP-USP16 NLS (Tag)-N and GFP-USP16 were all generated by PCR-based subcloning into either the pENTR D-Topo plasmid or modified Myc-pENTR D-Topo plasmid. USP16 Δ CD1, USP16 Δ CD2, USP16 Δ N-term, USP16 Δ C-term and USP16 Δ NES were generated by subcloning with annealed short adaptors into pENTR D-Topo USP16 plasmid or modified Myc-pENTR D-Topo plasmid. USP16 CD1-M and USP16 CD2-M ubiquitin-binding mutants were generated by subcloning synthetic fragments containing N200A/D299A/E302A/S376A/E380A or E644A/L646A/K682AR699A/F700A/K709A/H750A/Y759A, respectively. Both mutants were inserted into pENTR D-Topo USP16 plasmid or modified Myc-pENTR D-Topo plasmid. USP16 Δ Linker NLS (Tag) was generated by subcloning annealed NLS of SV40 large T antigen (Tag) sequence adaptors into the pENTR D-Topo USP16 Δ Linker plasmid. All USP16 expression constructs were generated using the USP16 siRNA-resistant plasmid. The pENTR D-Topo plasmids or modified Myc-pENTR D-Topo plasmids were recombined using LR clonase kit (Life Technologies) into pDEST-Myc plasmid or pLenti-CMV vector (17452, Addgene), respectively. pOD35 GFP 1-9 (USP16), pOD35 GFP NLS (USP16) and pOD35 GFP NLS (Tag) were generated by subcloning annealed oligonucleotides into the pOD35 plasmid (provided by Dr. Paul Maddox (Institute for Research in Immunology and Cancer, Canada). GFP-Linker, GFP-Linker-NLS (Tag), GFP 685-708, GFP 150-185, GFP-P1 (460-540), GFP-P2 (541-618), GFP-P3 (460-508), GFP-P4 (509-563) and GFP-P5 (564-618) were generated by PCR-based

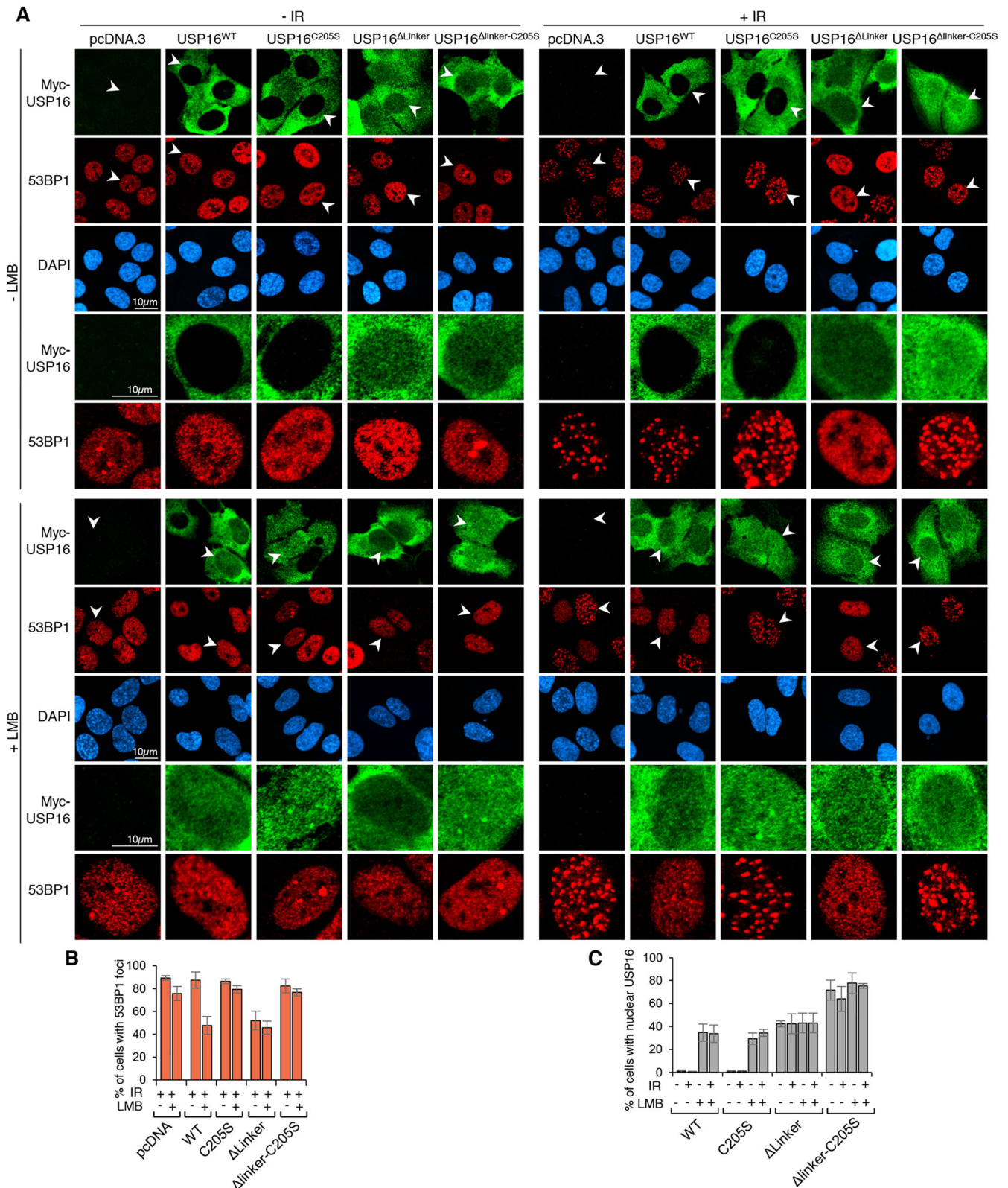


Fig. 8. Enforced nuclear accumulation of USP16 abolishes the assembly of DNA repair foci. (A) U2OS cells were transfected with either pcDNA, Myc-USP16 WT, Myc-USP16 C205S, Myc-USP16 Δ linker or Myc-USP16 Δ linker C205S expression vectors and subjected to different treatments (10 nM LMB and/or 7.5 Gy ionizing radiation). The subcellular localization of USP16 and the presence of 53BP1 foci were detected with the indicated antibodies. Arrowheads indicate the position of selected nuclei. (B) Cell counts from experiments performed as indicated in A showing the percentage of cells harboring 53BP1 foci in presence of Myc-USP16 or the corresponding mutants. Note that 53BP1 foci were counted automatically based on the whole-cell population of transfected and non-transfected cells. The results are presented as mean \pm s.d.; $n=4$ biological replicates. (C) Cell counts from experiments performed as indicated in A showing the nuclear localization of USP16 in transfected cells following LMB and/or ionizing radiation treatments. More than 100 cells were counted in four independent experiments and values are presented as mean \pm s.d.

subcloning fragments of USP16 into the pEGFP-N3 plasmid. GFP-NES (HIV1 Rev), and additional USP16 fragments, GFP-P6 (572-586), GFP-P7 (585-597), GFP-P8 (604-618), GFP-301-313 and GFP-374-392 were generated by subcloning of the corresponding annealed short adaptors into the pEGFP-N3 plasmid. All constructs were verified by sequencing.

Cell culture, transient transfections and treatments

U2OS osteosarcoma (ATCC, HTB-96) and HEK293T human embryonic kidney cells (ATCC, CRL-3216) were grown in Dulbecco's modified Eagle's medium (DMEM, Life Technologies) containing 5% new born calf serum (NBS), 1% L-glutamine and 1% penicillin/streptomycin. Normal human lung IMR90 fibroblasts (ATCC, CCL-186) were grown in DMEM containing 10% fetal bovine serum (FBS), 1% L-glutamine and 1% penicillin/streptomycin. DNA plasmids were transfected into U2OS cells using Lipofectamine 2000 (Life Technologies). HEK293T cells were transfected using polyethylenimine (PEI) (Sigma-Aldrich). At 3 days post transfection, cells were treated with 10 nM leptomycin B (LMB) (cat. #9676S, Cell Signaling Technology), 200 ng/ml nocodazole (cat. #487928, Millipore-Sigma), 10 μ M CDK1 inhibitor RO-3306 (cat. #217699, Millipore-Sigma) or 2 mM thymidine (cat. #T9250, Millipore-Sigma) and harvested for western blotting, flow cytometry or immunostaining. For DNA repair studies, at 3 days post-transfection, U2OS cells were incubated with or without 10 nM LMB for 24 h, exposed to 7.5 Gy ionizing radiation (IR) and then collected at the indicated time points for immunostaining. The cell lines used were tested negative for mycoplasma contamination, using DAPI staining. Cell lines obtained from ATCC were initially amplified in large quantities and then frozen to avoid extended culture. Cell morphology and proliferation rates were always checked.

Viral transduction and generation of cell lines stably expressing wild-type or mutant USP16

U2OS or IMR90 cells stably expressing wild-type or mutant USP16 were generated by lentiviral gene delivery. HEK293T cells were transfected with pLenti-CMV USP16 or mutant plasmids with the packaging vectors psPAX2 (12260, Addgene) and pMD2-G (12259, Addgene). Lentivirus particles were collected and used to transduce cells twice followed by 48 h of puromycin selection (2 μ g/ml). The pooled cell populations were used for localization studies within 1 month after selection.

siRNA-induced protein depletion and CRISPR/Cas9-mediated gene knockout

Four siRNA oligonucleotides targeting human USP16 and two siRNA oligonucleotides targeting human Ring1A or Ring1B were purchased from Sigma-Aldrich (Table S3) and pooled as indicated for transfection in U2OS cells using Lipofectamin RNAimax (Life Technologies). USP16 gRNA sequences (21 bp oligonucleotides) were generated using the <https://bio.tools/chopchop> and <https://cm.jefferson.edu/Off-Spotter/> programs to exclude potential off-targets (Table S3). These sequences were synthesized by Biobasic Inc., annealed and cloned into the pLentiCRISPR_V2 plasmid (52961, Addgene). We used the pLentiCRISPR_V2 empty vector as a control. Lentiviruses were generated by transfection in HEK293T cells as described above. Media containing lentivirus particles were used to infect U2OS cells twice. Pooled populations of USP16-knockout cells were selected for 48 h by treatment with puromycin (2 μ g/ml) and the USP16 depletion efficiency assessed by western blotting.

Immunofluorescence

The procedure was carried essentially as previously described (Daou et al., 2011). Briefly, U2OS cells plated on coverslips were treated as indicated, fixed using 3% PFA and permeabilized with PBS solution containing 0.5% NP-40. Non-specific sites were blocked with PBS with 0.1% NP-40 supplemented with 10% FBS. The coverslips were then incubated with mouse monoclonal and/or rabbit polyclonal primary antibodies. Anti-rabbit-IgG conjugated to Alexa Fluor[®] 594 and anti-mouse-IgG conjugated to Alexa Fluor[®] 488 (Life Technologies) were used as secondary antibodies. Nuclei were stained with DAPI. Cell membranes were stained on live cells with Alexa Fluor[™] 594-conjugated wheat germ agglutinin (WGA) (cat. # W11262, Life Technologies). The cells were observed using imager Zeiss

Z2 microscope equipped with Plan-Apochromat 63 \times 1.4 NA and 100 \times 1.4 NA Oil DIC objectives and an AxioCam MRm camera. Cells were also observed with an inverted confocal fluorescence microscope (Olympus FV1000 LSM) with a 60 \times oil immersion objective lens. Collected images were processed using WCIF-ImageJ program (NIH) and red-green-blue (RGB) profiles were generated (Schneider et al., 2012). Z-stacks were acquired using an inverted confocal fluorescence microscope (Olympus FV1000 LSM) with a 60 \times oil immersion objective lens. Live cell epifluorescence images were obtained using a LX71 Olympus microscope, with a 60 \times oil immersion objective, 1.35NA. Automatic time lapse imaging was performed using an in-house LabVIEW program (Binan et al., 2016).

Cell counts of USP16 subcellular localization and fluorescence signal determination

The subcellular localization of USP16 was determined by counting the relevant cell population groups for each experiment. For Fig. 2B, C2TA is either evenly distributed between the cytoplasm and the nucleus or predominantly nuclear. USP16 is either localized in the cytoplasm or found in both the cytoplasm and nucleus, with no predominant staining in the nucleus. Data is presented for each cell population as the percentage of the total cells expressing C2TA or USP16. For Figs 2D,G, 3C, 6B, 7F and 8C, Figs S2E, S3D, S4D, S5B, S5F and S6D, USP16 is localized either in the cytoplasm or in both the cytoplasm and nucleus. Thus, we counted all cells with a nuclear staining of USP16 (signal distinctly above background) and reported their percentage relative to all transfected cells counted. For Figs 4B, 5C,G, USP16 is cytoplasmic, mostly cytoplasmic but with nuclear staining, evenly distributed between the cytoplasm and the nucleus, mostly nuclear but with cytoplasmic staining or predominantly nuclear. These cell populations were counted, and data is presented as percentage of the total cells expressing USP16. To consolidate cell counts, whenever possible, we also monitored the decrease of H2Aub signal as an indicator of USP16 nuclear accumulation. For Figs 1B,C and 3A, Figs S1C, S3B and S5D, quantification of USP16 signals in the nucleus and cytoplasm was conducted using ImageJ software. The background signal was taken from cell-free areas and subtracted from cytoplasmic or nuclear signals. The measurement of these signals was conducted on 10 cells and data is presented as mean \pm s.d.

Overall, the experiments were repeated more than three times to ensure data reproducibility. No particular sample size calculation was done. We did not exclude data unless a major technical problem justified the exclusion. Results in panels represent mean \pm s.d. for at least three independent experiments.

Synchronization and cell cycle analysis

Transfected or infected U2OS cells were synchronized at G2/M or late G2 following 24 h treatment with 200 ng/ml nocodazole (Hammond-Martel et al., 2010) or 10 μ g/ml CDK1 inhibitor (RO-3306) (Daou et al., 2018), respectively. Mitotic cells were enriched using nocodazole treatment, harvested by shake-off, and released from metaphase arrest to enter G1 after replating in nocodazole-free medium. The remaining population of adherent cells was enriched in G2, but also contained a fraction of M cells that resisted shake-off, and this mixed population and was considered as G2/M. G1/S cells were enriched using a thymidine double-block protocol and then released toward S (Daou et al., 2015). Cells were fixed for immunostaining as described above or used for cell cycle analysis. Flow cytometry analysis (FACS) was conducted as described previously (Hammond-Martel et al., 2010). Cells were harvested by trypsinization and fixed using PBS containing 75% (v/v) ethanol. Cells were then treated with 100 μ g/ml RNase A and stained with 50 μ g/ml propidium iodide. DNA content was analyzed using a FACScan flow cytometer fitted with the CellQuestPro software (BD Biosciences).

Immunoblotting

Total cell extracts were obtained by cell lysis with in a buffer containing 25 mM Tris-HCl pH 7.3 and 1% SDS. Cell extracts were boiled at 95 $^{\circ}$ C for 10 min and then sonicated and used for western blotting. Total proteins were quantified using the bicinchoninic acid (BCA) assay, and then diluted in Laemmli buffer. For western blotting, the band signals were obtained with a

LAS-3000 LCD camera coupled to the MultiGauge software (Fuji, Stamford, CT). All immunoblotting data for analysis of protein expression is displayed as Fig. S8.

Subcellular fractionation

Nuclear and cytoplasmic fractions were obtained following hypotonic cell lysis. Briefly, semi-confluent dishes were washed twice and incubated for 5 min with hypotonic lysis buffer containing 10 mM Tris-HCl pH 7.3, 10 mM KCl, 1.5 mM MgCl₂, 10 mM β-Mercaptoethanol, 1 mM PMSF and protease inhibitors cocktail (Sigma-Aldrich). Cells were then scraped, resuspended and lysed using a dounce homogenizer. Cytoplasmic and nuclear fractions were obtained after centrifugation at 1700 *g* for 15 min. Total cell fractions were harvested directly in the hypotonic buffer and completed to 1% SDS. To minimize cross contaminations, nuclear pellets were resuspended in 3 ml of sucrose buffer S1 (0.1 M sucrose and 10 mM MgCl₂) and layered over a 3 ml sucrose cushion S2 (0.35 M sucrose, 0.5 mM MgCl₂) by slowly pipetting S1 solution on top of S2. These sucrose cushions were centrifuged at 1500 *g* for 10 min. The sucrose was then removed, and the purified nuclear fractions were resuspended in hypotonic buffer containing 1% SDS.

Protein co-immunoprecipitation

HEK293T cells were transfected with the indicated expression constructs and immunoprecipitation conducted as previously described (Daou et al., 2018).

Labeling with DUB activity probes

U2OS cells expressing various mutants of USP16 were harvested in PBS. Following centrifugation (1700 *g* for 5 min), cell pellets were resuspended in 1:10 (v/v) ratio in 50 mM Tris-HCl pH 7.3, 100 mM NaCl, 5 mM MgCl₂, 2.5 mM DTT, 2 mM ATP, 0.1% Igepal, 1 mM PMSF and protease inhibitors cocktail. Following incubation for 20 min on ice, the cell extracts were centrifuged at 25,200 *g* for 8 min and 20 μl of cell lysates were incubated with 20 μl of buffer with 1 μl of HA-tagged ubiquitin-VME or ubiquitin-Br DUB activity probes (Borodovsky et al., 2001, 2002). After 2 h incubation at 37°C, cells were added 40 μl of sample buffer and used for immunoblotting detection of USP16.

Protein sequences alignment, motifs prediction and structure modeling

USP16 domains were analyzed using ExPASy from the SIB Bioinformatics Resource Portal (<http://www.expasy.org/>) (Artimo et al., 2012). NLS and NES predictions was undertaken using the NLStradamus (Nguyen Ba et al., 2009) and NetNES servers (la Cour et al., 2004), respectively. Multiple alignments of USP16 orthologs were performed using Aline (Bond and Schuttelkopf, 2009) or Geneious created by Biomatters (available from <http://www.geneious.com>) as described in the figure legends. According to a sequence similarity, a homology model of USP16 NES in complex with CRM1 was generated from the crystal structure of PKI NES in complex with CRM1–Ran RanBP1 (PDB 3NBY). The USP16 NES was modeled by manually replacing PKI amino acids (GSLNELALKLGLDI) with USP16 amino acids (GEVDISNGFKNLNL) using Coot (Emsley et al., 2010).

A homology model of the USP16 catalytic domain was generated using SWISS Model (<https://swissmodel.expasy.org/>). The structural model comprises both parts of the catalytic domain (CD1 and CD2) without the intermediate loop (amino acids from G197 to S394 and A615 to L823). A structural model of the USP16 catalytic domain in complex with ubiquitin was obtained by superimposition of the obtained USP16 catalytic domain homology model with the crystal structure of either USP2 (PDB 2HD5) or USP7 (PDB 1NBF) both in complex with ubiquitin. Structural figures showing USP16 NES, USP16 catalytic domain homology model as well as the polar interactions between USPs and ubiquitin were generated by PyMol (Schrodinger, LLC. 2010. The PyMOL Molecular Graphics System, Version 1.8.0.5).

Acknowledgements

We thank Diana Adjaoud, Djaleb Abdelhadi, Antoine Simoneau and Emilie Allard for technical assistance and Saad Mengaad for his help with image assembly.

Competing interests

The authors declare no competing or financial interests.

Author contributions

Conceptualization: N.S.N., E.B.A.; Methodology: N.S.N., S.D., M.U., J.G., N.V.I., H.B., H.Y., L.M., E.F., N.Z.C., N.M., L.B., M.S., F.B., S.C., E.B.A.; Software: N.S.N., S.D., M.U., J.G., N.V.I., H.B., H.Y., L.M., E.F., N.Z.C., N.M., L.B., M.S., F.B., E.B.A.; Validation: N.S.N., S.D., M.U., J.G., N.V.I., H.B., H.Y., L.M., E.F., N.Z.C., N.M., L.B., M.S., F.B., E.B.A.; Formal analysis: N.S.N., S.D., M.U., J.G., N.V.I., H.B., H.Y., L.M., E.F., N.Z.C., N.M., L.B., M.S., F.B., E.B.A.; Investigation: N.S.N., S.D., M.U., J.G., N.V.I., H.B., L.M., E.F., N.Z.C., N.M., M.S., F.B., E.B.A.; Resources: N.S.N., E.B.A.; Data curation: N.S.N., S.D., E.B.A.; Writing - original draft: N.S.N., E.B.A.; Writing - review & editing: N.S.N., S.D., M.U., E.D., E.M., H.W., S.C., E.B.A.; Visualization: N.S.N., S.D., E.D., E.M., H.W., S.C., E.B.A.; Supervision: N.S.N., E.B.A.; Project administration: E.B.A.; Funding acquisition: E.B.A.

Funding

This work was supported by a discovery grant (2015-2021) to E.B.A. from The Natural Sciences and Engineering Research Council of Canada (NSERC), a discovery grant (2013-2019) to H.W. from NSERC, a discovery grant (2018-2023) to E.M. from NSERC and a discovery grant (2016-2021) to S.C. from NSERC. H.W., S.C. and E.B.A. are Scholars of Fonds de la Recherche en Santé (FRQ-S). J.G. was supported by a Master's scholarship from the FRQ-S. N.S.N. was supported by a PhD scholarship from the FRQ-S. N.M. was supported by a PhD scholarship from Fonds de Recherche du Québec-Nature et Technologies (FRQ-NT). H.Y. was supported by a PhD scholarship from the CIHR.

Supplementary information

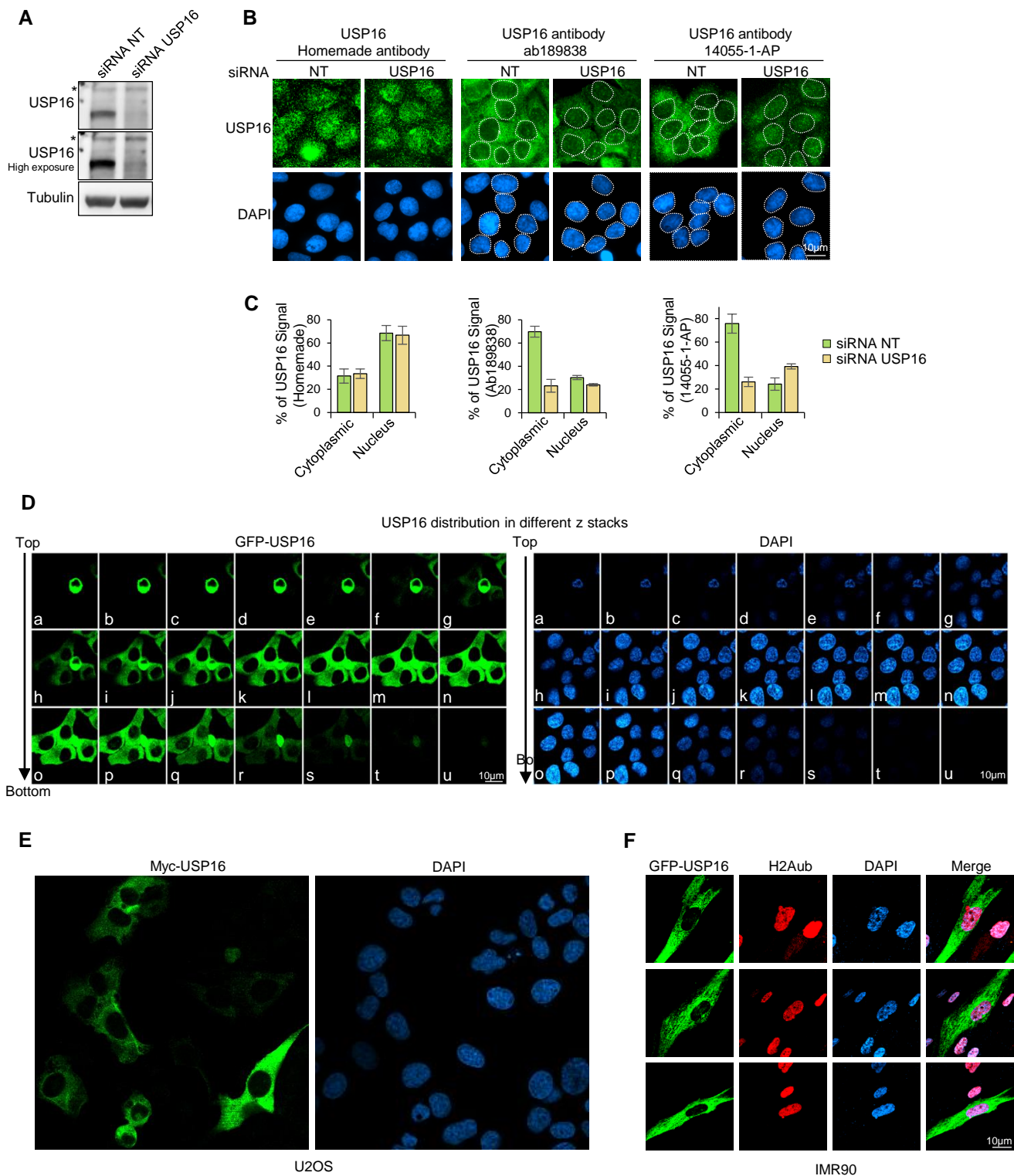
Supplementary information available online at <http://jcs.biologists.org/lookup/doi/10.1242/jcs.239236.supplemental>

References

- Adorno, M., Sikandar, S., Mitra, S. S., Kuo, A., Nicolis Di Robilant, B., Haro-Acosta, V., Ouadah, Y., Quarta, M., Rodriguez, J., Qian, D. et al. (2013). Usp16 contributes to somatic stem-cell defects in Down's syndrome. *Nature* **501**, 380-384. doi:10.1038/nature12530
- Artimo, P., Jonnalagedda, M., Arnold, K., Baratin, D., Csardi, G., de Castro, E., Duvaud, S., Flegel, V., Fortier, A., Gasteiger, E. et al. (2012). ExPASy: SIB bioinformatics resource portal. *Nucleic Acids Res.* **40**, W597-W603. doi:10.1093/nar/gks400
- Binan, L., Mazzaferri, J., Choquet, K., Lorenzo, L.-E., Wang, Y.C., Affar, E.B., De Koninck, Y., Ragoussis, J., Kleinman, C.L. and Costantinos, S. (2016). Live single-cell laser tag. *Nat. Commun.* **7**, 11636. doi:10.1038/ncomms11636
- Bonacci, T., Suzuki, A., Grant, G. D., Stanley, N., Cook, J. G., Brown, N. G. and Emanuele, M. J. (2018). Cezanne/OTUD7B is a cell cycle-regulated deubiquitinase that antagonizes the degradation of APC/C substrates. *EMBO J.* **37**, e98701. doi:10.15252/embj.201798701
- Bond, C. S. and Schuttelkopf, A. W. (2009). ALINE: a WYSIWYG protein-sequence alignment editor for publication-quality alignments. *Acta Crystallogr. D Biol. Crystallogr.* **65**, 510-512. doi:10.1107/S0907444909007835
- Borodovsky, A., Kessler, B. M., Casagrande, R., Overkleef, H. S., Wilkinson, K. D. and Ploegh, H. L. (2001). A novel active site-directed probe specific for deubiquitylating enzymes reveals proteasome association of USP14. *EMBO J.* **20**, 5187-5196. doi:10.1093/emboj/20.18.5187
- Borodovsky, A., Ovaa, H., Kolli, N., Gan-Erdene, T., Wilkinson, K. D., Ploegh, H. L. and Kessler, B. M. (2002). Chemistry-based functional proteomics reveals novel members of the deubiquitinating enzyme family. *Chem. Biol.* **9**, 1149-1159. doi:10.1016/S1074-5521(02)00248-X
- Cai, S.-Y., Babbitt, R. W. and Marchesi, V. T. (1999). A mutant deubiquitinating enzyme (Ubp-m) associates with mitotic chromosomes and blocks cell division. *Proc. Natl. Acad. Sci. USA* **96**, 2828-2833. doi:10.1073/pnas.96.6.2828
- Clague, M. J., Herd, C. and Urbé, S. (2015). The demographics of the ubiquitin system. *Trends Cell Biol.* **25**, 417-426. doi:10.1016/j.tcb.2015.03.002
- Clague, M. J., Urbé, S. and Komander, D. (2019). Breaking the chains: deubiquitylating enzyme specificity begets function. *Nat. Rev. Mol. Cell Biol.* **20**, 338-352. doi:10.1038/s41580-019-0099-1
- Cressman, D. E., O'Connor, W. J., Greer, S. F., Zhu, X.-S. and Ting, J. P. (2001). Mechanisms of nuclear import and export that control the subcellular localization of class II transactivator. *J. Immunol.* **167**, 3626-3634. doi:10.4049/jimmunol.167.7.3626
- Daou, S., Mashtalir, N., Hammond-Martel, I., Pak, H., Yu, H., Sui, G., Vogel, J. L., Kristie, T. M. and Affar, E. B. (2011). Crosstalk between O-GlcNAcylation and proteolytic cleavage regulates the host cell factor-1 maturation pathway. *Proc. Natl. Acad. Sci. USA* **108**, 2747-2752. doi:10.1073/pnas.1013822108
- Daou, S., Hammond-Martel, I., Mashtalir, N., Barbour, H., Gagnon, J., Iannantuono, N. V. G., Nkwe, N. S., Motorina, A., Pak, H., Yu, H. et al. (2015). The BAP1/ASXL2 histone H2A deubiquitinase complex regulates cell

- proliferation and is disrupted in cancer. *J. Biol. Chem.* **290**, 28643-28663. doi:10.1074/jbc.M115.661553
- Daou, S., Barbour, H., Ahmed, O., Masclef, L., Baril, C., Sen Nkwe, N., Tchelougou, D., Uriarte, M., Bonnel, E., Ceccarelli, D. et al.** (2018). Monoubiquitination of ASXLs controls the deubiquitinase activity of the tumor suppressor BAP1. *Nat. Commun.* **9**, 4385. doi:10.1038/s41467-018-06854-2
- Eletr, Z. M. and Wilkinson, K. D.** (2014). Regulation of proteolysis by human deubiquitinating enzymes. *Biochim. Biophys. Acta* **1843**, 114-128. doi:10.1016/j.bbamcr.2013.06.027
- Emsley, P., Lohkamp, B., Scott, W. G. and Cowtan, K.** (2010). Features and development of Coot. *Acta Crystallogr. D Biol. Crystallogr.* **66**, 486-501. doi:10.1107/S0907444910007493
- Esmaili, A. M., Johnson, E. L., Thaivalappil, S. S., Kuhn, H. M., Kornbluth, S. and Iruela, P. M.** (2010). Regulation of the ATM-activator protein Avn by CRM1-dependent nuclear export. *Cell Cycle* **9**, 3913-3920. doi:10.4161/cc.9.19.13138
- Frail, J. M., Quesada, V., Rodríguez, D., Freije, J. M. and Lopez-Otin, C.** (2012). Deubiquitinases in cancer: new functions and therapeutic options. *Oncogene* **31**, 2373-2388. doi:10.1038/onc.2011.443
- Frangini, A., Sjöberg, M., Roman-Trufero, M., Dharmalingam, G., Haberle, V., Bartke, T., Lenhard, B., Malumbres, M., Vidal, M. and Dillon, N.** (2013). The aurora B kinase and the polycomb protein ring1B combine to regulate active promoters in quiescent lymphocytes. *Mol. Cell* **51**, 647-661. doi:10.1016/j.molcel.2013.08.022
- Fu, S. C., Imai, K. and Horton, P.** (2011). Prediction of leucine-rich nuclear export signal containing proteins with NESsential. *Nucleic Acids Res.* **39**, e111. doi:10.1093/nar/gkr493
- Fung, H. Y., Fu, S. C. and Choek, Y. M.** (2017). Nuclear export receptor CRM1 recognizes diverse conformations in nuclear export signals. *Elife* **6**, e23961. doi:10.7554/eLife.23961.046
- García-Santisteban, I., Bañuelos, S. and Rodríguez, J. A.** (2012). A global survey of CRM1-dependent nuclear export sequences in the human deubiquitinase family. *Biochem. J.* **441**, 209-217. doi:10.1042/BJ20111300
- Gelsi-Boyer, V., Trouplin, V., Adelaide, J., Aceto, N., Remy, V., Pinson, S., Houdayer, C., Arnoulet, C., Sainty, D., Bentires-Alj, M. et al.** (2008). Genome profiling of chronic myelomonocytic leukemia: frequent alterations of RAS and RUNX1 genes. *BMC Cancer* **8**, 299. doi:10.1186/1471-2407-8-299
- Gomez-Diaz, C. and Ikeda, F.** (2018). Roles of ubiquitin in autophagy and cell death. *Semin. Cell Dev. Biol.* **93**, 125-135. doi:10.1016/j.semdb.2018.09.004
- Grumati, P. and Dikic, I.** (2018). Ubiquitin signaling and autophagy. *J. Biol. Chem.* **293**, 5404-5413. doi:10.1074/jbc.TM117.000117
- Gu, Y., Jones, A. E., Yang, W., Liu, S., Dai, Q., Liu, Y., Swindle, C. S., Zhou, D., Zhang, Z., Ryan, T. M. et al.** (2016). The histone H2A deubiquitinase Usp16 regulates hematopoiesis and hematopoietic stem cell function. *Proc. Natl. Acad. Sci. USA* **113**, E51-E60. doi:10.1073/pnas.1517041113
- Hammond-Martel, I., Pak, H., Yu, H., Rouget, R., Horwitz, A. A., Parvin, J. D., Drobetsky, E. A. and Affar, E. B.** (2010). PI 3 kinase related kinases-independent proteolysis of BRCA1 regulates Rad51 recruitment during genotoxic stress in human cells. *PLoS ONE* **5**, e14027. doi:10.1371/journal.pone.0014027
- Hammond-Martel, I., Yu, H. and Affar, E. B.** (2012). Roles of ubiquitin signaling in transcription regulation. *Cell. Signal.* **24**, 410-421. doi:10.1016/j.cellsig.2011.10.009
- Harper, J. W., Ordeu, A. and Heo, J.-M.** (2018). Building and decoding ubiquitin chains for mitophagy. *Nat. Rev. Mol. Cell Biol.* **19**, 93-108. doi:10.1038/nrm.2017.129
- Heaton, S. M., Borg, N. A. and Dixit, V. M.** (2016). Ubiquitin in the activation and attenuation of innate antiviral immunity. *J. Exp. Med.* **213**, 1-13. doi:10.1084/jem.20151531
- Hu, H. and Sun, S.-C.** (2016). Ubiquitin signaling in immune responses. *Cell Res.* **26**, 457-483. doi:10.1038/cr.2016.40
- Jackson, S. P. and Durocher, D.** (2013). Regulation of DNA damage responses by ubiquitin and SUMO. *Mol. Cell* **49**, 795-807. doi:10.1016/j.molcel.2013.01.017
- Joo, H.-Y., Zhai, L., Yang, C., Nie, S., Erdjument-Bromage, H., Tempst, P., Chang, C. and Wang, H.** (2007). Regulation of cell cycle progression and gene expression by H2A deubiquitination. *Nature* **449**, 1068-1072. doi:10.1038/nature06256
- Julien, C., Coulombe, P. and Meloche, S.** (2003). Nuclear export of ERK3 by a CRM1-dependent mechanism regulates its inhibitory action on cell cycle progression. *J. Biol. Chem.* **278**, 42615-42624. doi:10.1074/jbc.M302724200
- Komander, D., Clague, M. J. and Urbé, S.** (2009). Breaking the chains: structure and function of the deubiquitinases. *Nat. Rev. Mol. Cell Biol.* **10**, 550-563. doi:10.1038/nrm2731
- Kosugi, S., Hasebe, M., Matsumura, N., Takashima, H., Miyamoto-Sato, E., Tomita, M. and Yanagawa, H.** (2009). Six classes of nuclear localization signals specific to different binding grooves of importin α . *J. Biol. Chem.* **284**, 478-485. doi:10.1074/jbc.M807017200
- la Cour, T., Kiemer, L., Molgaard, A., Gupta, R., Skriver, K. and Brunak, S.** (2004). Analysis and prediction of leucine-rich nuclear export signals. *Protein Eng. Des. Sel.* **17**, 527-536. doi:10.1093/protein/gzh062
- Lange, A., Mills, R. E., Lange, C. J., Stewart, M., Devine, S. E. and Corbett, A. H.** (2007). Classical nuclear localization signals: definition, function, and interaction with importin alpha. *J. Biol. Chem.* **282**, 5101-5105. doi:10.1074/jbc.R600026200
- Liu, J. and DeFranco, D. B.** (2000). Protracted nuclear export of glucocorticoid receptor limits its turnover and does not require the exportin 1/CRM1-directed nuclear export pathway. *Mol. Endocrinol.* **14**, 40-51. doi:10.1210/mend.14.1.0398
- Mashtair, N., Daou, S., Barbour, H., Sen, N. N., Gagnon, J., Hammond-Martel, I., Dar, H. H., Therrien, M. and Affar, E. B.** (2014). Autodeubiquitination protects the tumor suppressor BAP1 from cytoplasmic sequestration mediated by the atypical ubiquitin ligase UBE2O. *Mol. Cell* **54**, 392-406. doi:10.1016/j.molcel.2014.03.002
- Mendler, L., Braun, T. and Müller, S.** (2016). The ubiquitin-like SUMO system and heart function: from development to disease. *Circ. Res.* **118**, 132-144. doi:10.1161/CIRCRESAHA.115.307730
- Meivissen, T. E. T. and Komander, D.** (2017). Mechanisms of deubiquitinase specificity and regulation. *Annu. Rev. Biochem.* **86**, 159-192. doi:10.1146/annurev-biochem-061516-044916
- Mimnaugh, E. G., Kayastha, G., McGovern, N. B., Hwang, S.-G., Marcu, M. G., Trepel, J., Cai, S.-Y., Marchesi, V. T. and Neckers, L.** (2001). Caspase-dependent deubiquitination of monoubiquitinated nucleosomal histone H2A induced by diverse apoptogenic stimuli. *Cell Death Differ.* **8**, 1182-1196. doi:10.1038/sj.cdd.4400924
- Murai, N., Murakami, Y. and Matsufuji, S.** (2003). Identification of nuclear export signals in antizyme-1. *J. Biol. Chem.* **278**, 44791-44798. doi:10.1074/jbc.M308059200
- Nguyen Ba, A. N., Pogoutse, A., Provart, N. and Moses, A. M.** (2009). NLStradamus: a simple hidden markov model for nuclear localization signal prediction. *BMC Bioinformatics* **10**, 202. doi:10.1186/1471-2105-10-202
- Nijman, S. M. B., Luna-Vargas, M. P., Velds, A., Brummelkamp, T. R., Dirac, A. M., Sixma, T. K. and Bernards, R.** (2005). A genomic and functional inventory of deubiquitinating enzymes. *Cell* **123**, 773-786. doi:10.1016/j.cell.2005.11.007
- Nishi, R., Wijnhoven, P., le Sage, C., Tjeertes, J., Galanty, Y., Forment, J. V., Clague, M. J., Urbé, S. and Jackson, S. P.** (2014). Systematic characterization of deubiquitinating enzymes for roles in maintaining genome integrity. *Nat. Cell Biol.* **16**, 1016-1026. doi:10.1038/ncb3028
- Panier, S. and Boulton, S. J.** (2014). Double-strand break repair: 53BP1 comes into focus. *Nat. Rev. Mol. Cell Biol.* **15**, 7-18. doi:10.1038/nrm3719
- Perrody, E., Abrami, L., Feldman, M., Kunz, B., Urbé, S. and van der Goot, F. G.** (2016). Ubiquitin-dependent folding of the Wnt signaling coreceptor LRP6. *Elife* **5**, e19083. doi:10.7554/eLife.19083.018
- Popovic, D., Vucic, D. and Dikic, I.** (2014). Ubiquitination in disease pathogenesis and treatment. *Nat. Med.* **20**, 1242-1253. doi:10.1038/nm.3739
- Reyes-Turcu, F. E., Horton, J. R., Mullaly, J. E., Heroux, A., Cheng, X. and Wilkinson, K. D.** (2006). The ubiquitin binding domain ZnF UBP recognizes the C-terminal diglycine motif of unanchored ubiquitin. *Cell* **124**, 1197-1208. doi:10.1016/j.cell.2006.02.038
- Reyes-Turcu, F. E., Ventii, K. H. and Wilkinson, K. D.** (2009). Regulation and cellular roles of ubiquitin-specific deubiquitinating enzymes. *Annu. Rev. Biochem.* **78**, 363-397. doi:10.1146/annurev.biochem.78.082307.091526
- Rodier, G., Montagnoli, A., Di Marcotullio, L., Coulombe, P., Draetta, G. F., Pagano, M. and Meloche, S.** (2001). p27 cytoplasmic localization is regulated by phosphorylation on Ser10 and is not a prerequisite for its proteolysis. *EMBO J.* **20**, 6672-6682. doi:10.1093/emboj/20.23.6672
- Rubinsztein, D. C.** (2006). The roles of intracellular protein-degradation pathways in neurodegeneration. *Nature* **443**, 780-786. doi:10.1038/nature05291
- Sahtoe, D. D. and Sixma, T. K.** (2015). Layers of DUB regulation. *Trends Biochem. Sci.* **40**, 456-467. doi:10.1016/j.tibs.2015.05.002
- Schneider, C. A., Rasband, W. S. and Eliceiri, K. W.** (2012). NIH Image to ImageJ: 25 years of image analysis. *Nat. Methods* **9**, 671-675. doi:10.1038/nmeth.2089
- Schwertman, P., Bekker-Jensen, S. and Mailand, N.** (2016). Regulation of DNA double-strand break repair by ubiquitin and ubiquitin-like modifiers. *Nat. Rev. Mol. Cell Biol.* **17**, 379-394. doi:10.1038/nrm.2016.58
- Senft, D., Qi, J. and Ronai, Z. A.** (2018). Ubiquitin ligases in oncogenic transformation and cancer therapy. *Nat. Rev. Cancer* **18**, 69-88. doi:10.1038/nrc.2017.105
- Shanbhag, N. M., Rafalska-Metcalf, I. U., Balane-Bolivar, C., Janicki, S. M. and Greenberg, R. A.** (2010). ATM-dependent chromatin changes silence transcription in cis to DNA double-strand breaks. *Cell* **141**, 970-981. doi:10.1016/j.cell.2010.04.038
- Soniat, M. and Choek, Y. M.** (2015). Nuclear localization signals for four distinct karyopherin- β nuclear import systems. *Biochem. J.* **468**, 353-362. doi:10.1042/BJ20150368
- Tanaka, K. and Matsuda, N.** (2014). Proteostasis and neurodegeneration: the roles of proteasomal degradation and autophagy. *Biochim. Biophys. Acta* **1843**, 197-204. doi:10.1016/j.bbamcr.2013.03.012
- Uckelmann, M. and Sixma, T. K.** (2017). Histone ubiquitination in the DNA damage response. *DNA Repair* **56**, 92-101. doi:10.1016/j.dnarep.2017.06.011
- Urbé, S., Liu, H., Hayes, S. D., Heride, C., Rigden, D. J. and Clague, M. J.** (2012). Systematic survey of deubiquitinase localization identifies USP21 as a regulator of centrosome- and microtubule-associated functions. *Mol. Biol. Cell* **23**, 1095-1103. doi:10.1091/mbc.e11-08-0668
- Vassilev, L. T., Tovar, C., Chen, S., Knezevic, D., Zhao, X., Sun, H., Heimbrook, D. C. and Chen, L.** (2006). Selective small-molecule inhibitor reveals critical mitotic functions of human CDK1. *Proc. Natl. Acad. Sci. USA* **103**, 10660-10665. doi:10.1073/pnas.0600447103

- Vucic, D., Dixit, V. M. and Wertz, I. E.** (2011). Ubiquitylation in apoptosis: a post-translational modification at the edge of life and death. *Nat. Rev. Mol. Cell Biol.* **12**, 439-452. doi:10.1038/nrm3143
- Wang, Z., Zhang, H., Liu, J., Cheruiyot, A., Lee, J.-H., Ordog, T., Lou, Z., You, Z. and Zhang, Z.** (2016). USP51 deubiquitylates H2AK13,15ub and regulates DNA damage response. *Genes Dev.* **30**, 946-959. doi:10.1101/gad.271841.115
- Werner, A., Manford, A. G. and Rape, M.** (2017). Ubiquitin-dependent regulation of stem cell biology. *Trends Cell Biol.* **27**, 568-579. doi:10.1016/j.tcb.2017.04.002
- Wertz, I. E. and Dixit, V. M.** (2010). Regulation of death receptor signaling by the ubiquitin system. *Cell Death Differ.* **17**, 14-24. doi:10.1038/cdd.2009.168
- Xu, Y., Yang, H., Joo, H. Y., Yu, J. H., Smith, A. D. T., Schneider, D., Chow, L. T., Renfrow, M. and Wang, H.** (2013). Ubp-M serine 552 phosphorylation by cyclin-dependent kinase 1 regulates cell cycle progression. *Cell Cycle* **12**, 3219-3227. doi:10.4161/cc.26278
- Yang, W., Lee, Y.-H., Jones, A. E., Woolnough, J. L., Zhou, D., Dai, Q., Wu, Q., Giles, K. E., Townes, T. M. and Wang, H.** (2014). The histone H2A deubiquitinase Usp16 regulates embryonic stem cell gene expression and lineage commitment. *Nat. Commun.* **5**, 3818. doi:10.1038/ncomms4818
- Yau, R. and Rape, M.** (2016). The increasing complexity of the ubiquitin code. *Nat. Cell Biol.* **18**, 579-586. doi:10.1038/ncb3358
- Zhang, Z., Yang, H. and Wang, H.** (2014). The histone H2A deubiquitinase USP16 interacts with HERC2 and fine-tunes cellular response to DNA damage. *J. Biol. Chem.* **289**, 32883-32894. doi:10.1074/jbc.M114.599605
- Zheng, N. and Shabek, N.** (2017). Ubiquitin ligases: structure, function, and regulation. *Annu. Rev. Biochem.* **86**, 129-157. doi:10.1146/annurev-biochem-060815-014922
- Zhuo, X., Guo, X., Zhang, X., Jing, G., Wang, Y., Chen, Q., Jiang, Q., Liu, J. and Zhang, C.** (2015). Usp16 regulates kinetochore localization of Plk1 to promote proper chromosome alignment in mitosis. *J. Cell Biol.* **210**, 727-735. doi:10.1083/jcb.201502044
- Zimmermann, M. and de Lange, T.** (2014). 53BP1: pro choice in DNA repair. *Trends Cell Biol.* **24**, 108-117. doi:10.1016/j.tcb.2013.09.003



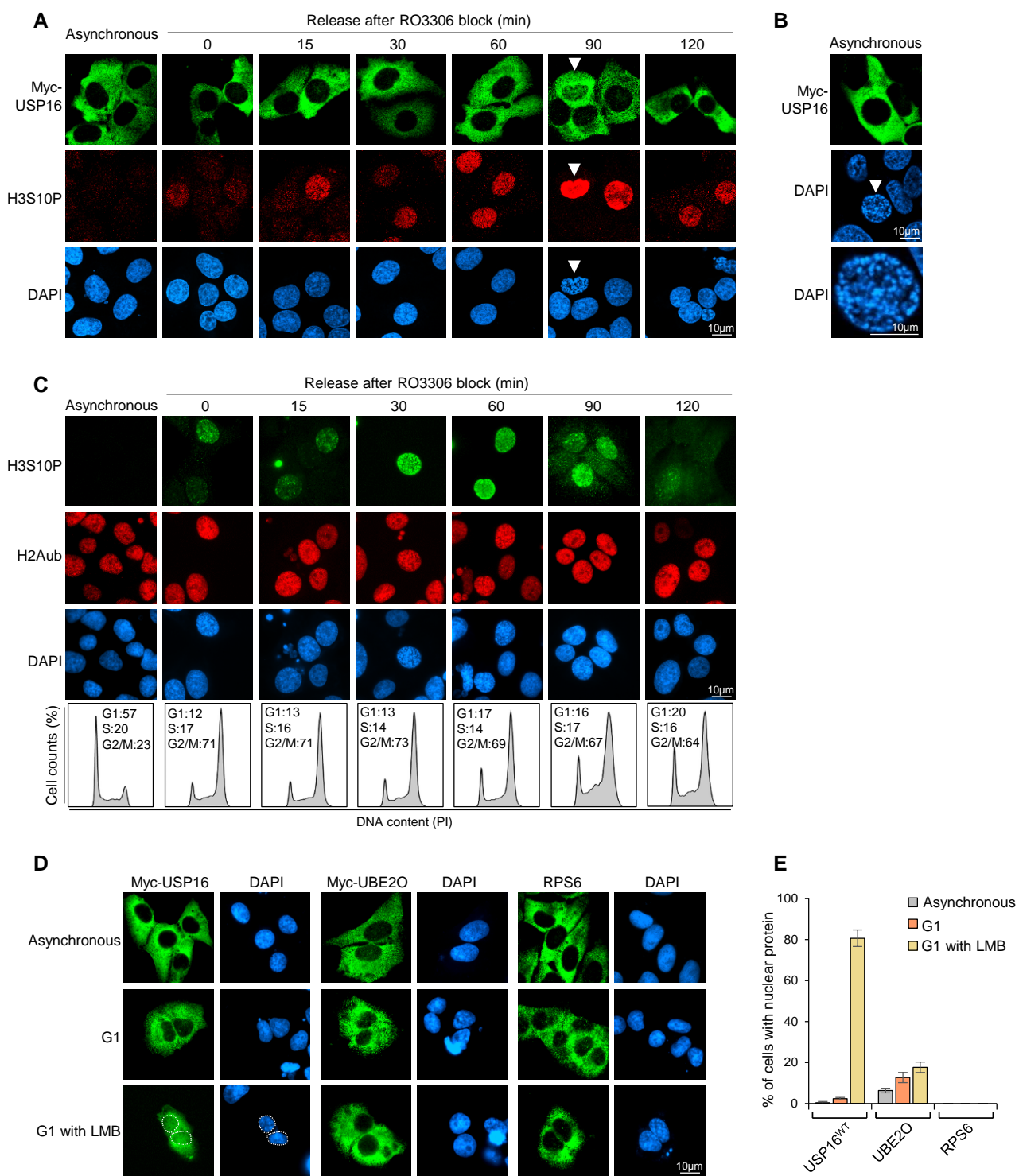
Supplementary Figure S1

Figure S1.

USP16 is localized in the cytoplasm in interphase.

(A) Specificity of immunoblotting of USP16 using our homemade antibody. U2OS cells were transfected with non-target control (NT) or USP16 siRNAs for 72 hours. USP16 was detected by immunoblotting on total cell extracts. Tubulin was used as a loading control. The blots of USP16 correspond to two exposure times during chemiluminescence detection. The stars indicate non-specific bands or possible modified forms of USP16. n= 5 biological replicates.

(B) U2OS cells were transfected with control (NT) or USP16 siRNAs for 72 hours. USP16 distribution was analyzed by immunofluorescence using homemade or commercial antibodies. **(C)** RGB profiles for the stainings were generated using ImageJ and relative quantification of the fluorescence signal in the nucleus versus cytoplasm was conducted. Data is presented as the percentage of fluorescence signal in each compartment versus total signal and corresponds to an average quantification on 10 cells \pm SD. n= 2 biological replicates **(D)** U2OS cells stably expressing GFP-USP16 were used for fluorescence detection. Images were collected at regular intervals to create a stack in the Z axis using a confocal microscope. **(E)** U2OS cells stably expressing Myc-USP16 were used for fluorescence detection. Images were collected using a confocal microscope. n= 5 biological replicates **(F)** IMR90 cells stably expressing GFP-USP16 were fixed and the sub-cellular localization of USP16 was determined by fluorescence microscopy. Immunofluorescence detection of H2Aub was also conducted. n= 3 biological replicates.

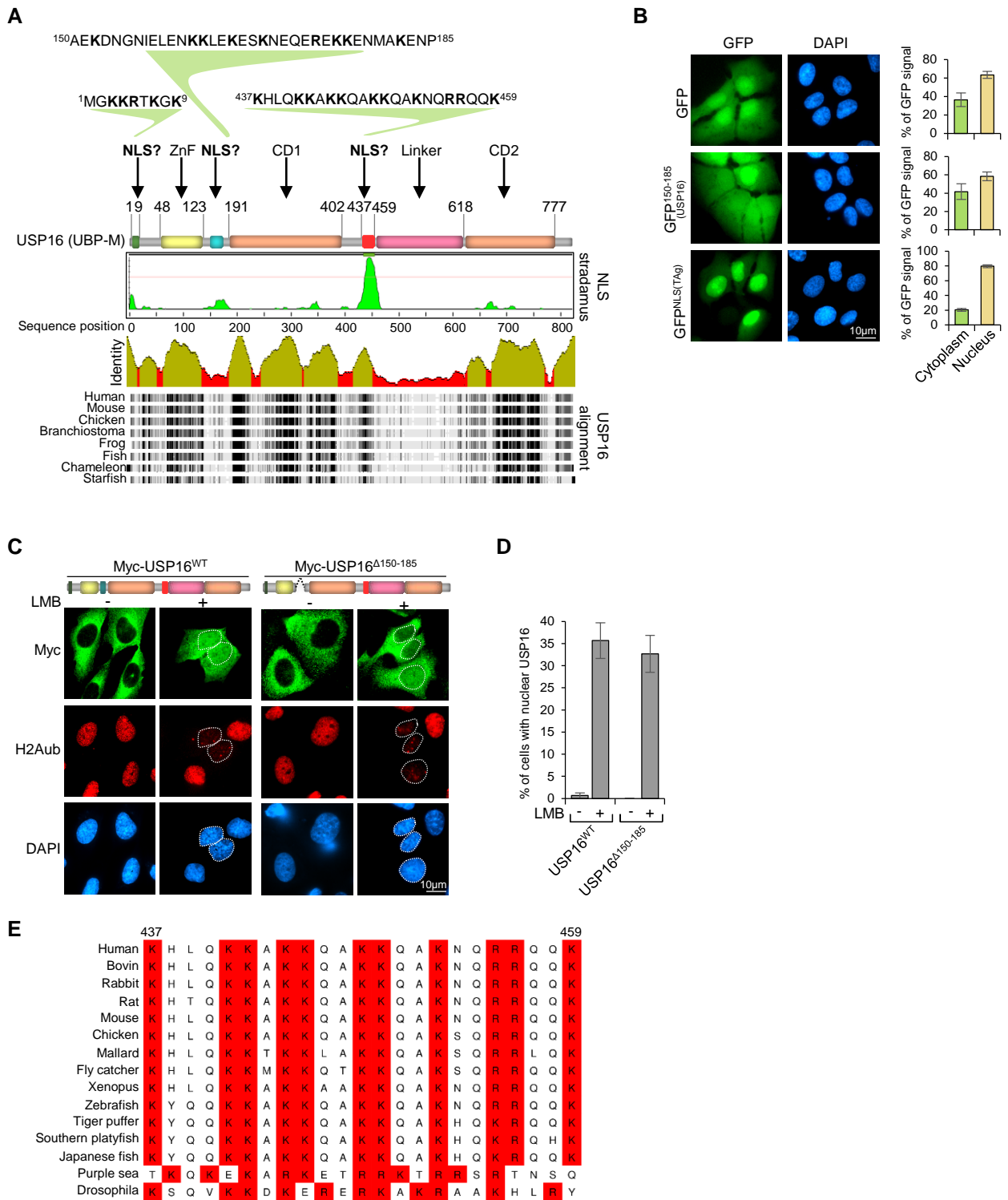


Supplementary Figure S2

Figure S2.

USP16 is transiently retained in the nucleus after mitosis.

(A) USP16 is not detected in the nucleus following cell cycle arrest in G2 and during progression towards mitosis. U2OS cells stably expressing Myc-USP16 were enriched in G2 phase with 10 μ M of RO3306 treatment and released at selected time points. USP16 sub-cellular localization and the levels of H3S10P were determined by immunofluorescence as indicated. Note that H3S10P staining could be readily observed, but without a distinct accumulation of USP16 in the nucleus. The arrow indicates a cell starting mitosis. $n=3$ biological replicates. (B) USP16 is not detected in the nucleus during chromosome condensation. The arrow indicates a nucleus starting chromosome condensation. (C) U2OS cells stably expressing Myc-USP16 were enriched in G2 phase with 10 μ M of RO3306 treatment and released at selected times. The levels of H2Aub and H3S10P were determined by immunofluorescence as indicated. The cell cycle profiles were analyzed by propidium iodide staining and FACS (Bottom panels). $n=3$ biological replicates. (D) U2OS cells were transfected with pDEST Myc-USP16 WT or pDEST Myc-UBE2O for three days. Cells were then synchronized with nocodazole and then released in the absence or presence of 10 nM of LMB for 5 hours. The sub-cellular localization of USP16 or UBE2O as well as endogenous Ribosomal Protein S6 (RPS6) was determined by immunofluorescence as indicated. No cells with nuclear RPS6 were observed. (E) Cell counts from experiments performed as indicated in panel D showing the nuclear localization of the indicated proteins. The results are from 3 independent experiments and the values are presented as average \pm SD.

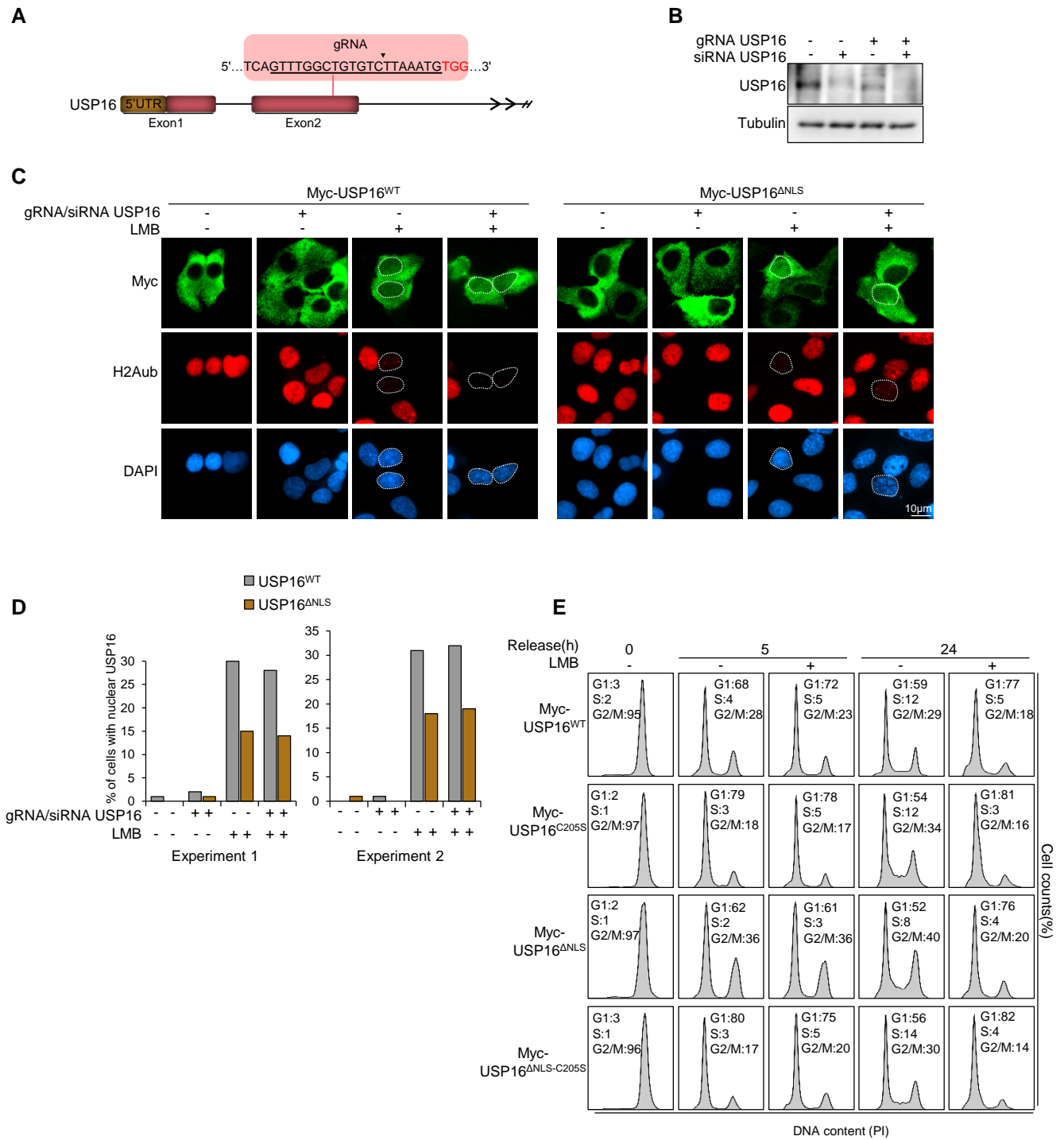


Supplementary Figure S3

Figure S3.

Identification of USP16 NLS.

(A) Prediction of NLS sequences in USP16. NLS sequences predictions were done with NLStradamus prediction software. The main functional domains of USP16 as well as the predicted NLS peptides are indicated. Multiple sequences alignment of USP16 across different species is also shown. (B) The 150-185 amino acid sequence of USP16 is not sufficient to target GFP to the nucleus. pEGFP N3, GFP N3 150-185(USP16) and pOD35 GFP NLS (TA_g) constructs were transfected in U2OS and sub-cellular localization of fusion proteins was detected by fluorescence. T antigen NLS was included as a positive control. Relative quantification of GFP signal in the nucleus versus cytoplasm was conducted on 10 cells and data is presented as average \pm SD. n= 3 biological replicates. (C) Deletion of the 150-185 amino acid sequence of USP16 does not perturb its localization with or without LMB treatment. U2OS cells stably expressing Myc-USP16^{WT} or Myc-USP16 ^{Δ 150-185} were treated with 10 nM of LMB for 24 hours. Sub-localization was determined by immunofluorescence with the indicated antibodies. n= 3 biological replicates. (D) Cell counts of USP16 nuclear localization from experiments performed as indicated in panel C. The results are from three independent experiments and the values are presented as average \pm SD. n= 3 biological replicates. (E) Conservation of USP16 NLS. Sequence alignments of USP16 orthologs. The alignment was performed with Aline using different sequences of USP16 obtained from Uniprot. The lysine and arginine residues forming the NLS are highlighted in red.

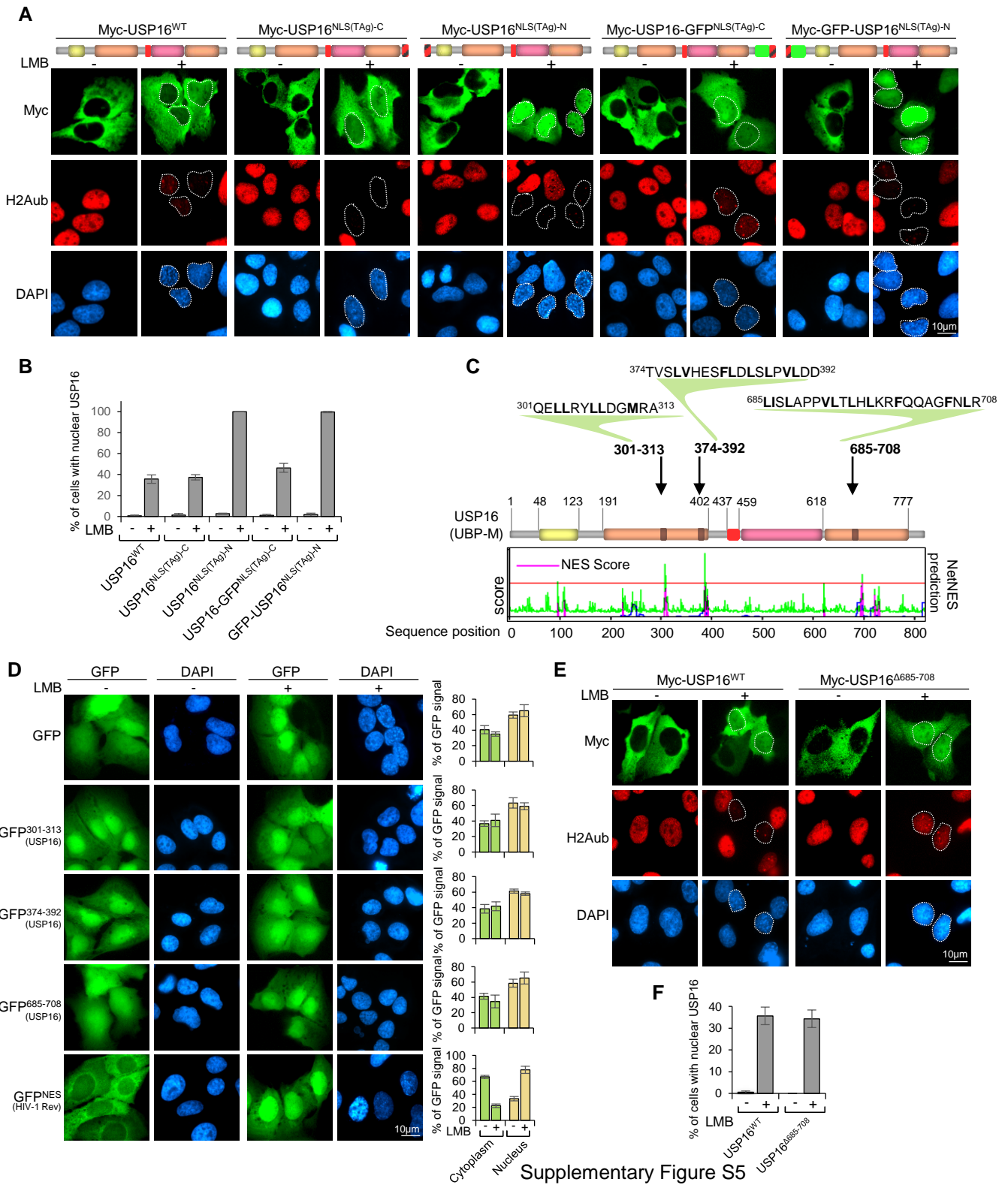


Supplementary Figure S4

Figure S4.

Localization of USP16 lacking its NLS in the absence of endogenous USP16.

(A) Graphical representation of USP16 gene and the gRNA sequence used for CRISPR/Cas9 targeting. (B) Depletion of USP16 using CRISPR/Cas9 and RNAi approaches. U2OS cells were transfected with USP16 siRNA for 72 hours or infected with CRISPR/Cas9 lentiviruses targeting USP16. U2OS cells were also infected with CRISPR/Cas9 lentiviruses and then subjected to siRNA for 72 hours and then used for USP16 detection by immunoblotting as indicated. Tubulin was used as a loading control. n= 2 biological replicates. (C) U2OS cells stably expressing Myc-USP16^{WT} or Myc-USP16^{ΔNLS} were infected with CRISPR/Cas9 lentivirus particles with gRNA targeting USP16. Cells were then also transfected with USP16 siRNA for 72 hours to obtain a strong reduction of USP16 in the majority of the cell population. Cells were then treated with 10 nM LMB for 24 hours and used for immunofluorescence as indicated. (D) Cell counts from two experiments performed as indicated in panel C showing nuclear localization of USP16 and its corresponding mutants. More than 100 cells were counted in each condition. n= 2 biological replicates. (E) The cell cycle profile of each population from Figure 4 panel A was analyzed by propidium iodide staining and FACS.

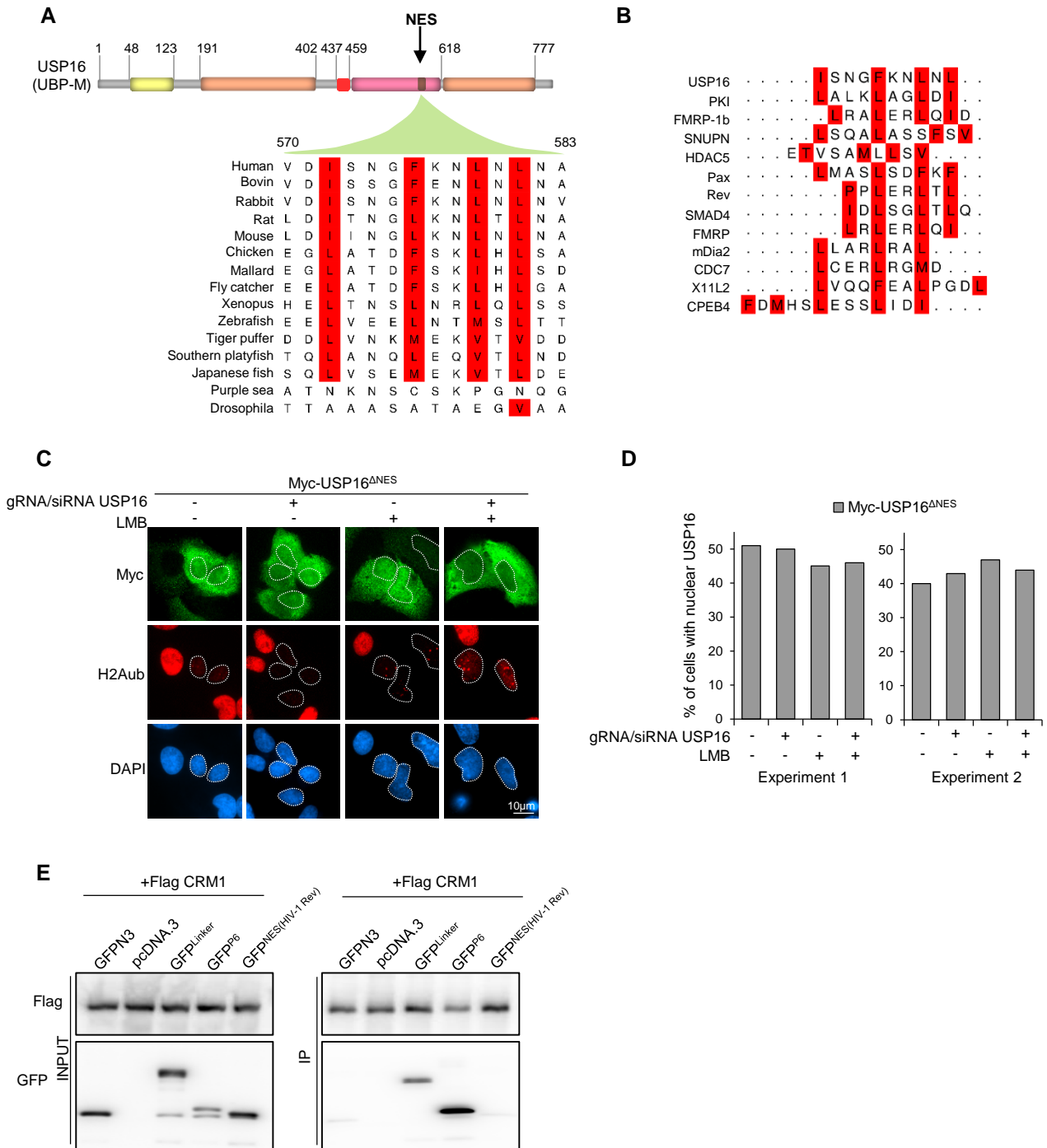


Supplementary Figure S5

Figure S5.

Identification of USP16 nuclear export signal.

(A) U2OS cells expressing Myc-USP16^{WT}, Myc-USP16^{NLS(TAg)-C}, Myc-USP16^{NLS(TAg)-N}, USP16-GFP^{NLS(TAg)-C} or USP16-GFP^{NLS(TAg)-N} were treated with 10 nM of LMB for 24 hours. Sub-cellular localization was determined by immunofluorescence using the indicated antibodies. Schematic representation of the different USP16 constructs are shown. n= 3 biological replicates. (B) Cell counts from experiments performed as indicated in panel A showing sub-cellular localization of USP16 and its corresponding mutants. More than 100 cells were counted in each condition. The results are from 3 independent experiments and the values are presented as average \pm SD. (C) NES sequences predictions were done with NetNES 1.1 Server prediction software. The colored lines correspond to different probability score values and the red line represents a probability threshold. The main functional domains of USP16 as well as the predicted NES sequences are shown. (D) U2OS cells were transfected with pEGFP N3, GFP-301-313 (USP16), GFP-374-392 (USP16), GFP-685-708 (USP16) or GFP-NES (HIV-1 Rev) expression constructs. Cells were treated with 10 nM of LMB and sub-cellular localization of these GFP-fusion proteins was determined by fluorescence. RGB profiles for GFP staining were generated using ImageJ and relative quantification of fluorescence signals in the nucleus and cytoplasm was conducted. Data is presented as the percentage of fluorescence signal in each compartment versus total signal and corresponds to the average measurements on 10 cells \pm SD. n= 3 biological replicates. (E) U2OS cells stably expressing USP16^{WT} or USP16 ^{Δ 685-708} were treated with LMB for 24 hours. The sub-cellular localization of USP16 was determined by immunofluorescence using the indicated antibodies. n= 3 biological replicates. (F) Cell counts from experiments performed as indicated in panel E showing the nuclear localization of USP16. The results are from 3 independent experiments and the values are presented as average \pm SD.

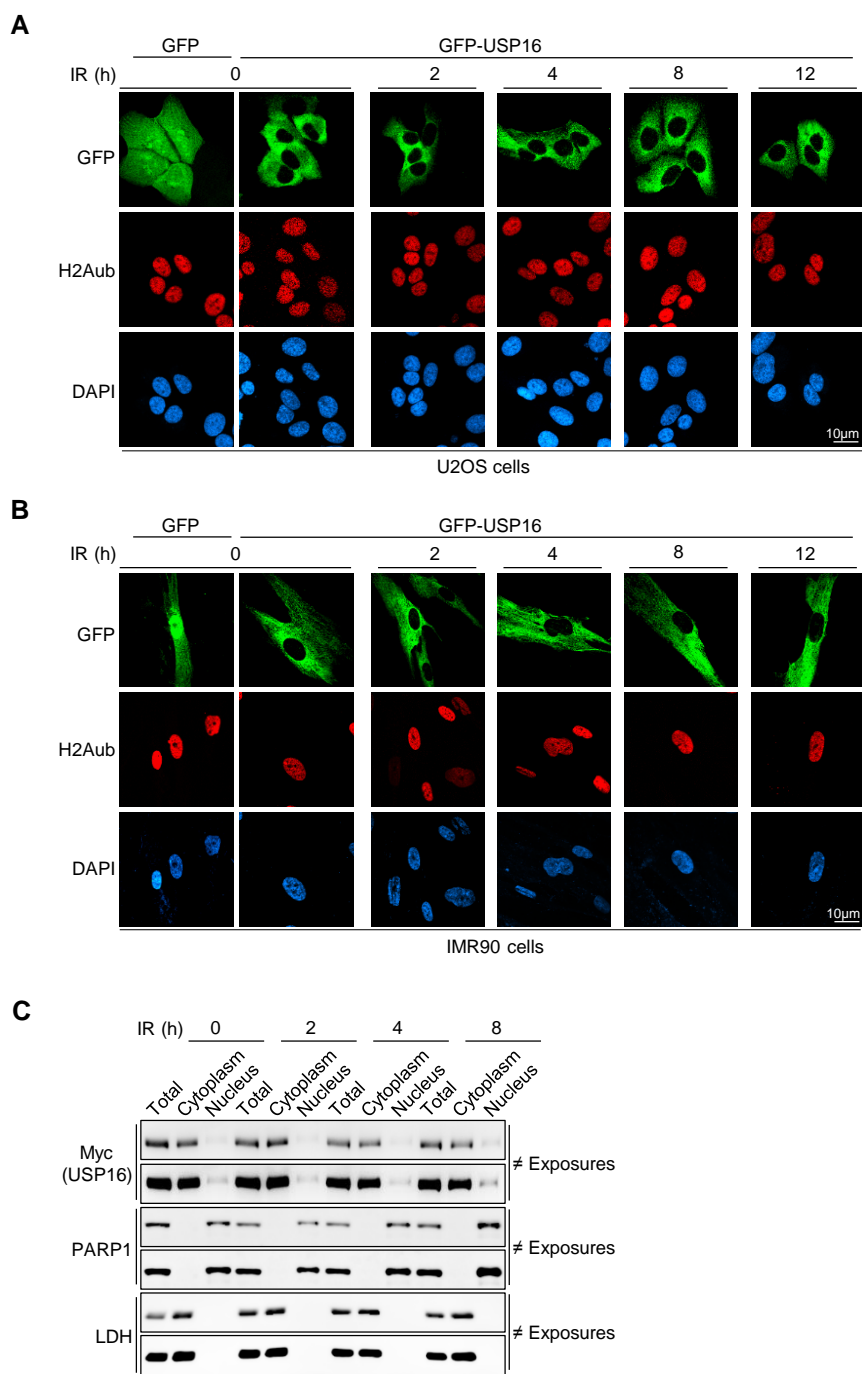


Supplementary Figure S6

Figure S6.

Localization of USP16 lacking its NES in the absence of endogenous USP16.

(A) Phylogenetic conservation of USP16 NES. Sequence conservation of the NES region of USP16 between different species. Sequences were obtained from Uniprot database and aligned using Aline software. The hydrophobic amino acids forming the NES are highlighted in red. (B) Sequence comparison of the NES region of USP16 with different NES sequences from different proteins. Sequence alignment was done with Aline. The hydrophobic amino acids forming USP16 and the current NES patterns are highlighted in red. (C) Localization of Myc-USP16^{ΔNES} following depletion of endogenous USP16. U2OS cells stably expressing Myc-USP16^{ΔNES} were infected with CRISPR/Cas9 lentiviral particles targeting USP16 and then transfected with USP16 siRNA for 72 hours. Cells were then treated with 10 nM of LMB for 24 hours. Sub-cellular localization was determined by immunofluorescence using the indicated antibodies. (D) Count from two experiments performed in C showing sub-cellular localization of Myc-USP16^{ΔNES}. At least 100 cells were counted for each condition. n= 2 biological replicates. (E) Interaction between USP16-NES and CRM1/ Exportin1. HEK293T cells were transfected with pEGFP N3, pcDNA, GFP-Linker, GFP-P6, GFP-NES (HIV-1 Rev) or Flag-CRM1 vectors and subjected to immunoprecipitation and immunoblotting. n= 2 biological replicates.

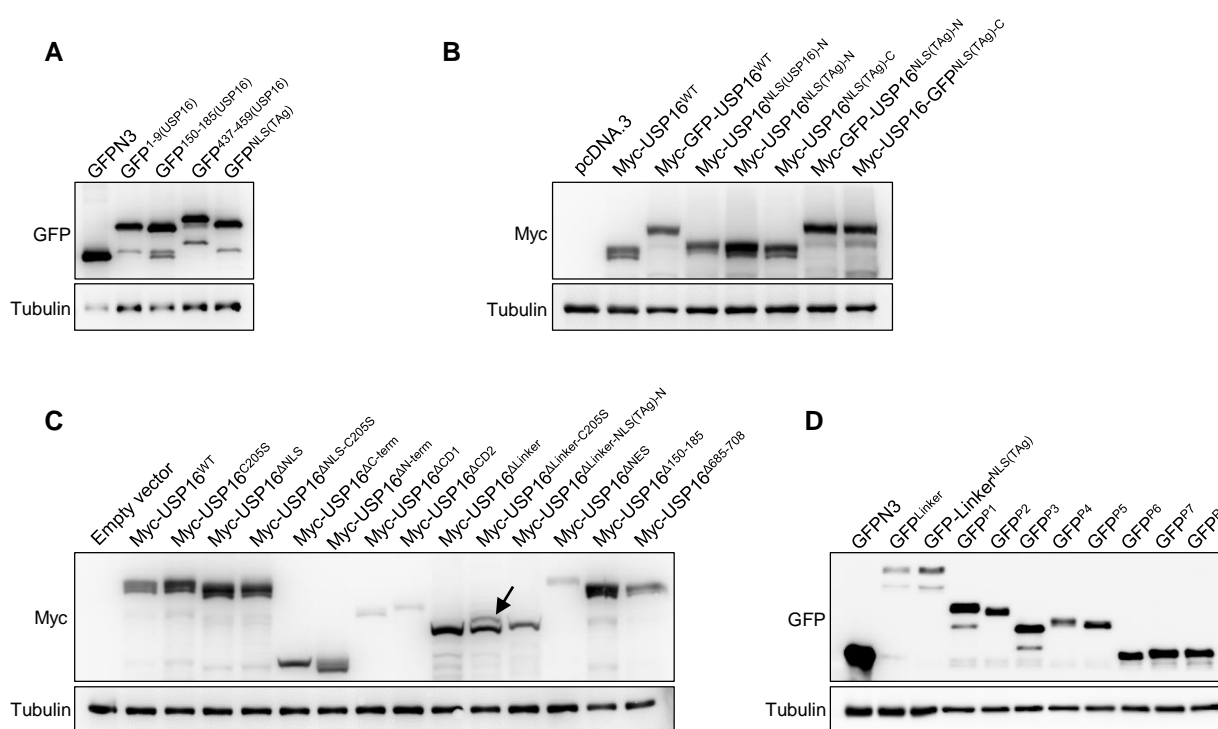


Supplementary Figure S7

Figure S7.

Ionizing radiation treatment does not induce USP16 nuclear translocation.

USP16 is not translocated into the nucleus during DNA damage by ionizing radiation. **(A)** U2OS cells stably expressing GFP-USP16 were irradiated with ionizing radiation (7,5 Gy). USP16 sub-cellular localization was determined by fluorescence as indicated. Cells expressing GFP were used as controls for transduction efficiency. **(B)** IMR90 cells stably expressing GFP-USP16 were treated and analyzed as in panel A. n= 2 biological replicates. **(C)** U2OS cells stably expressing Myc-USP16 were subjected to ionizing radiation (IR) (7,5 Gy) and harvested at the indicated time points for cell fractionation. Nuclear and cytoplasmic fractions were prepared at the indicated time points. PARP-1 and LDH were used as fractionation controls for nuclear and cytoplasmic fractions, respectively. n= 3 biological replicates.



Supplementary Figure S8

Figure S8.

Immunoblotting detection of protein expression for the constructs used in this study.

(A) U2OS cells were transfected with expression constructs encoding various GFP-peptide fusions. Three days post-transfection, cells were harvested for immunoblotting using anti-GFP antibody. n= 3 biological replicates. (B) U2OS cells were transfected with various expression constructs encoding fusions of USP16 with GFP and/or NLS sequences. Three days later, cells were harvested for immunoblotting using anti-Myc antibody. n= 3 biological replicates. (C) U2OS cells were transduced with viruses harboring expression constructs for various deletions or mutations in USP16. Two days later, cells were selected with puromycin for 48 hours and pools of cells stably expressing proteins were harvested for immunoblotting using anti-Myc antibody. n= 3 biological replicates. (D) U2OS cells were transfected with expression constructs encoding various GFP-peptide fusions. Three days post-transfection, cells were harvested for immunoblotting using anti-GFP antibody. α -Tubulin was used as a loading control. n= 3 biological replicates.

Table S1

List of antibodies used

Antibody	Source	Catalogue number	Dilution	Reference
Mouse monoclonal anti-Flag (M2)	Sigma-Aldrich	F3165	1:2000 (IF)	(Daou et al., 2018)
Mouse monoclonal anti-MYC	Covance	9E10	1:1000 (IF)	(Daou et al., 2018)
Homemade rabbit polyclonal anti-USP16	This study	NA	1:1000 (IF) 1:1000 (WB)	This study
Rabbit polyclonal anti-H2Aub K119 (D27C4)	Cell signaling	8240	1:5000 (IF) 1:10000 (WB)	(Daou et al., 2018)
Mouse monoclonal anti RPS6 (C8)	Santa Cruz	sc-74459	1:1000 (IF)	(Xie et al., 2019)
Mouse monoclonal anti-Tubulin (B-5-1-2)	Santa Cruz	sc-23948	1:2000 (WB)	(Daou et al., 2018)
Mouse monoclonal anti-PARP-1 (F-2)	Santa Cruz	sc-8007	1:2000 (WB)	(Hammond-Martel et al., 2010)
Mouse monoclonal anti-LDH (H-10)	Santa Cruz	sc-133123	1:1000 (WB)	(Daou et al., 2011)
Mouse monoclonal anti-Ring1B (N-32)	Santa Cruz	sc-101109	1:1000 (WB)	(Mashtalir et al., 2014)
Mouse monoclonal anti-Ubiquitin (P4D1)	Santa Cruz	sc-8017	1:500 (WB)	(Hammond-Martel et al., 2010)
Rabbit polyclonal anti-YY1 (H414)	Santa Cruz	sc-1703	1:1000 (WB)	(Daou et al., 2018)
Rabbit polyclonal anti-53BP1 (H300)	Santa Cruz	sc-22760	1:2000 (IF)	(Yu et al., 2014)
Rabbit polyclonal anti-USP16	Proteintech	14055-1-AP	1:500 (IF)	This study
Mouse monoclonal anti-phospho-H3 (Ser10) (3H10)	Millipore-Sigma	05-806	1:2000 (IF)	(Payton et al., 2018)
Rabbit polyclonal anti-phospho-H3 (Ser10)	Millipore-Sigma	06-570	1:1000 (IF)	(Teixeira et al., 2015)
Rabbit polyclonal anti-USP16	Abcam	ab189838	1:1000 (IF)	This study
Mouse anti-HA (home-made)	Homemade	NA	1:1000 (WB)	(Mashtalir et al., 2014)
Anti-mouse Alexa Fluor® 488	Life Technologies	A11029	1:1000 (IF)	(Daou et al., 2018)
Anti-rabbit Alexa Fluor® 594	Life Technologies	A11012	1:1000 (IF)	(Daou et al., 2018)
Alexa Fluor™ 594-conjugated wheat germ agglutinin (WGA)	Life Technologies	W11262	1:1000 (IF)	(Yamamoto et al., 2017)

Table S2: USP16 sequences

siRNA/gRNA resistant human USP16.

siRNA/gRNA resistant human USP16 was generated by gene synthesis. The USP16 cDNA sequence was manually modified using codon degeneracy.

[Click here to Download Table S2](#)

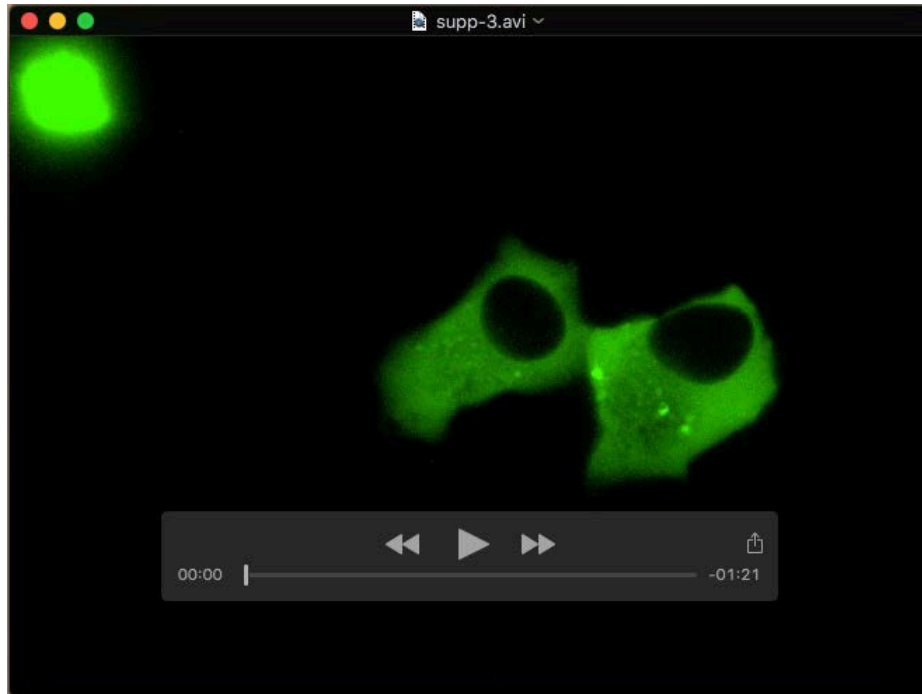
Table S3

siRNA / gRNA sequences

Target	Sequences		Name
hUSP16	siRNA_1	GGAUAAUGAUCUGGAGGUU	SASI_Hs01_00210893
	siRNA_2	GAAUGAUAGUCAUACUCCU	SASI_Hs01_00210894
	siRNA_3	GUGAAAGGAAGCAUGUUUA	SASI_Hs01_00210895
	siRNA_4	CCAAGAACCAACGAAGACA	SASI_Hs01_00210890
	gRNA_Foward	caccgGTTTGGCTGTGTCTTAAATG	N/A
	gRNA_Reverse	AaacCATTTAAGACACAGCCAAACC	N/A
hRing1A	siRNA_1	GAGUGUCCUACCUGCCGAA	SASI_Hs01_00058433
	siRNA_2	GGAAUACGAGGCCCAUCA	SASI_Hs01_00058434
	siRNA_3	CUAUCUGCCUGGACAUGGU	SASI_Hs01_00058435
	siRNA_4	CACAGAUUCUGCUCUGACU	SASI_Hs02_00334761
hRing1B	siRNA_1	CUAGUGAAAUUGAAUUAGU	SASI_Hs01_00213463
	siRNA_2	GACUACAAAGGAGUGUUUA	SASI_Hs01_00213464
	siRNA_3	GAAUGUCCUACCUGUCGGA	SASI_Hs01_00213465
	siRNA_4	GUUGAUCACUUAUCCAAGU	SASI_Hs02_00343201

REFERENCES

- Daou, S., H. Barbour, O. Ahmed, L. Masclef, C. Baril, N. Sen Nkwe, D. Tchelougou, M. Uriarte, E. Bonneil, D. Ceccarelli, N. Mashtalir, M. Tanji, J.Y. Masson, P. Thibault, F. Sicheri, H. Yang, M. Carbone, M. Therrien, and E.B. Affar. 2018. Monoubiquitination of ASXLs controls the deubiquitinase activity of the tumor suppressor BAP1. *Nat Commun.* 9:4385.
- Daou, S., N. Mashtalir, I. Hammond-Martel, H. Pak, H. Yu, G. Sui, J.L. Vogel, T.M. Kristie, and B. Affar el. 2011. Crosstalk between O-GlcNAcylation and proteolytic cleavage regulates the host cell factor-1 maturation pathway. *Proc Natl Acad Sci U S A.* 108:2747-2752.
- Hammond-Martel, I., H. Pak, H. Yu, R. Rouget, A.A. Horwitz, J.D. Parvin, E.A. Drobetsky, and B. Affar el. 2010. PI 3 kinase related kinases-independent proteolysis of BRCA1 regulates Rad51 recruitment during genotoxic stress in human cells. *PLoS One.* 5:e14027.
- Mashtalir, N., S. Daou, H. Barbour, N.N. Sen, J. Gagnon, I. Hammond-Martel, H.H. Dar, M. Therrien, and B. Affar el. 2014. Autodeubiquitination protects the tumor suppressor BAP1 from cytoplasmic sequestration mediated by the atypical ubiquitin ligase UBE2O. *Mol Cell.* 54:392-406.
- Payton, M., H.K. Cheung, M.S.S. Ninniri, C. Marinaccio, W.C. Wayne, K. Hanestad, J.D. Crispino, G. Juan, and A. Coxon. 2018. Dual Targeting of Aurora Kinases with AMG 900 Exhibits Potent Preclinical Activity Against Acute Myeloid Leukemia with Distinct Post-Mitotic Outcomes. *Mol Cancer Ther.* 17:2575-2585.
- Teixeira, L.K., X. Wang, Y. Li, S. Ekholm-Reed, X. Wu, P. Wang, and S.I. Reed. 2015. Cyclin E deregulation promotes loss of specific genomic regions. *Curr Biol.* 25:1327-1333.
- Xie, J., V. de Souza Alves, T. von der Haar, L. O'Keefe, R.V. Lenchine, K.B. Jensen, R. Liu, M.J. Coldwell, X. Wang, and C.G. Proud. 2019. Regulation of the Elongation Phase of Protein Synthesis Enhances Translation Accuracy and Modulates Lifespan. *Curr Biol.* 29:737-749 e735.
- Yamamoto, H., Y. Tobisawa, T. Inubushi, F. Irie, C. Ohyama, and Y. Yamaguchi. 2017. A mammalian homolog of the zebrafish transmembrane protein 2 (TMEM2) is the long-sought-after cell-surface hyaluronidase. *J Biol Chem.* 292:7304-7313.
- Yu, H., H. Pak, I. Hammond-Martel, M. Ghram, A. Rodrigue, S. Daou, H. Barbour, L. Corbeil, J. Hebert, E. Drobetsky, J.Y. Masson, J.M. Di Noia, and B. Affar el. 2014. Tumor suppressor and deubiquitinase BAP1 promotes DNA double-strand break repair. *Proc Natl Acad Sci U S A.* 111:285-290.



Movie 1.

USP16 is predominantly cytoplasmic during cell cycle progression.

U2OS cells were transfected with GFP-USP16 constructs and sub-cellular localization of USP16 was determined during cell cycle progression. Live cells fluorescence images were taken by 2 min time lapse for about 20 hours with a 60x oil immersion objective.